J. Electrochem. Sci. Eng. **16** (2026) 3045; https://doi.org/10.5599/jese.3045

Open Access : : ISSN 1847-9286
https://pub.iapchem.org/ojs/index.php/JESE

Review paper

Ultrasound-enhanced water electrolysis for hydrogen production: Mechanisms, metrology and energy metrics

Zeng ChenHongWen[1], Yew Heng Teoh[1,✉], Heoy Geok How[2], Mohamad Yusof Idroas[1] and Thanh Danh Le[3]

[1]*School of Mechanical Engineering, Universiti Sains Malaysia, Engineering Campus, Nibong Tebal 14300, Penang, Malaysia*
[2]*Department of Engineering, School of Engineering, Computing and Built Environment, UOW Malaysia KDU Penang University College, 32, Jalan Anson, 10400 Georgetown, Penang, Malaysia*
[3]*College of Technology and Design, University of Economics Ho Chi Minh City (UEH), 59C Nguyen Dinh Chieu Street, Xuan Hoa Ward, Ho Chi Minh City 700000, Viet Nam*

Corresponding Author: ✉*yewhengteoh@usm.my; Tel.: +604-5996325; Fax: +604-5941025*

Received: October 10, 2025; Revised: January 6, 2026; Published: January 20, 2026

Abstract

Ultrasound intensifies hydrogen production in water electrolysis cells by thinning boundary layers, accelerating bubble detachment, and, in tuned windows, modulating cavitation chemistry, yet cross-study claims remain difficult to compare. Focusing on ultrasound-enhanced water electrolysis (sono-electrolysis), this review aligns reporting with IEC 61161 (radiation-force acoustic power) and IEC 62127-2:2025 (hydrophone calibration); requires delivered acoustic intensity at the electrode, I_{del} / W·cm^{-2}, with stated traceability; pairs isothermal control with uncertainty budgets; and benchmarks performance using Δ-metrics: Δj (current-density gain at fixed cell voltage), Δη (cell voltage/overpotential reduction at fixed current density) and ΔHPR (hydrogen production rate gain at matched electrical input), together with specific energy consumption (SEC, kWh·kg^{-1} H_2). A window-based synthesis indicates that, under isothermal operation, 20 to 40 kHz with delivered intensity ≈0.2 to 1.0 W·cm^{-2} reproducibly yields Δj ≈ 15 to 30 %, Δη ≈ 40 to 120 mV, ΔHPR ≈ 10 to 30 %, and net SEC improvements of ~8 to 12 % when auxiliary loads are included, whereas at higher dose (I_{del} ≈ 1.0 to 1.6 W·cm^{-2}) non-uniform fields, cloud shielding, and heating can saturate or reverse benefits. To prevent metric conflation, hybrid sono-hydrogen routes are reviewed separately. The review concludes by proposing a minimum reporting set-frequency, waveform/duty and pulse repetition frequency, I_{del} (traceability/uncertainty), geometry/stand-off, electrolyte and dissolved gas, bulk temperature and runtime, gas metrology with temperature/pressure corrections, SEC boundaries and replicates/statistics, and by outlining priorities for operando cavitation-electrochemistry co-registration, geometry/void-fraction-aware scale-up, and durability under combined fields, to support reproducible, energy-accounted, and comparable studies across laboratories.

Keywords
Sono-electrolysis; acoustic cavitation; hybrid sono-hydrogen systems

Introduction

Hydrogen is a cross-cutting energy carrier for chemicals, heat, and power, yet scaling low-emissions supply via water electrolysis remains constrained by cost, durability, and infrastructure. Recent system-level assessments indicate a softening of project pipelines and slow conversion from announcements to firm capacity, with the cost gap to unabated fossil-based hydrogen persisting across most regions. These trends are documented in the IEA Global Hydrogen Review 2024 [1] and related updates, which also highlight that only a small fraction of announced projects has reached final investment decision and that electrolyser manufacturing must accelerate to meet 2030 targets [1]. Within this landscape, power ultrasound (US) offers a non-thermal intensification lever for water electrolysis systems.

Through acoustic cavitation, bubble growth and collapse generate microjets, acoustic streaming, and strong shear that (i) thin concentration boundary layers, (ii) enhance detachment of product bubbles, (iii) refresh and de-passivate reactive surfaces, and (iv) in tuned parameter windows, reduce apparent overpotential and transient cell voltage. Contemporary sonochemistry perspectives and cavitation-shear mini-reviews consolidate these mechanisms, while classical monographs provide the canonical basis for bubble dynamics and scaling arguments [2]. Applied to electrolytic hydrogen production, insonation can decrease bubble coverage and bubble-overpotential on the cathode, increasing instantaneous current density and, in some studies, reducing energy per unit H_2 at fixed production rate; frequency and waveform clearly matter (*e.g.* mechanistic HER investigations at 26 to 408 kHz) [3].

Crucially, benefits are not unconditional. When acoustic input power, and concomitant thermal rise, eclipses mass-transfer gains, net energy efficiency can decline. Recent design-of-experiments studies explicitly report cases where high-power insonation increased H_2 production rate yet lowered overall energy efficiency, underscoring the need for metrology-aware benchmarking rather than single-point snapshots [4]. To facilitate comparability and reproducibility, ultrasonic power and field characterization should follow recognized standards: IEC 61161 specifies radiation-force balance methods for calibrated acoustic power, and IEC 62127-2:2025 details absolute/relative hydrophone calibration for field mapping in water over 50 kHz to 100 MHz, both directly relevant to reporting delivered acoustic intensity at the electrode ($W \cdot cm^{-2}$), spatial non-uniformity and uncertainty budgets; national metrology institutes provide practical guidance on implementation and uncertainty evaluation [5-7]. Reactor-scale heterogeneity is another confounder: cavitation activity is highly non-uniform and depends on frequency, transducer geometry, loading, liquid height, and vessel architecture; mapping campaigns in multi-transducer reactors and systematic set-up analyses provide concrete protocols for field mapping and for interpreting scale-up artefacts [8].

To orient the reader, we first map where ultrasound fits in the low-emissions hydrogen landscape, linking the upstream system context to non-thermal mechanisms and to energy-normalized metrics, and delineate the scope adopted in this review (see Figure 1). Rather than surveying all hydrogen pathways, we focus on ultrasound-enhanced water electrolysis (sono-electrolysis) and centre the discussion on mechanisms, metrology, and comparable, energy-normalized metrics, and treat hybrid sono-hydrogen systems (*e.g.* sono- catalysis/photo-catalysis and other multi-field couplings) separately to avoid metric conflation; we compile parameter

windows (frequency, delivered intensity/power, temperature control, dissolved gases, continuous vs pulsed waveforms) and anchor reporting to specific energy consumption (SEC, kWh·kg^{-1} H_2) and Δ-metrics. Accordingly, this review addresses three questions: (RQ1) under isothermal, IEC-traceable acoustic dosing, defined as the quantification of delivered acoustic intensity or power at the electrode using IEC-compliant measurement protocols (*e.g.* IEC 61161 and IEC 62127-2), what reproducible ranges of Δ*j*, Δ*η* and ΔHPR can ultrasound deliver across alkaline (AEL) , proton exchange membrane (PEM), and anion exchange membrane (AEM) electrolyzer cells; (RQ2) within which frequency-intensity-temperature windows does ultrasound yield net gains in SEC once auxiliary loads are included; and (RQ3) what constitutes a minimum reporting set (MRS) that enables apples-to-apples benchmarking of sono-electrolysis (frequency; waveform, duty cycle, and pulse repetition frequency (PRF); delivered acoustic intensity at the electrode, I_{del}/W·cm^{-2}, with traceability; geometry/stand-off; electrolyte and dissolved gas; bulk temperature (*T*) and runtime; gas metrology with temperature/pressure (*T*/*P*) correction; SEC and Δ-metrics; replicates/statistics).

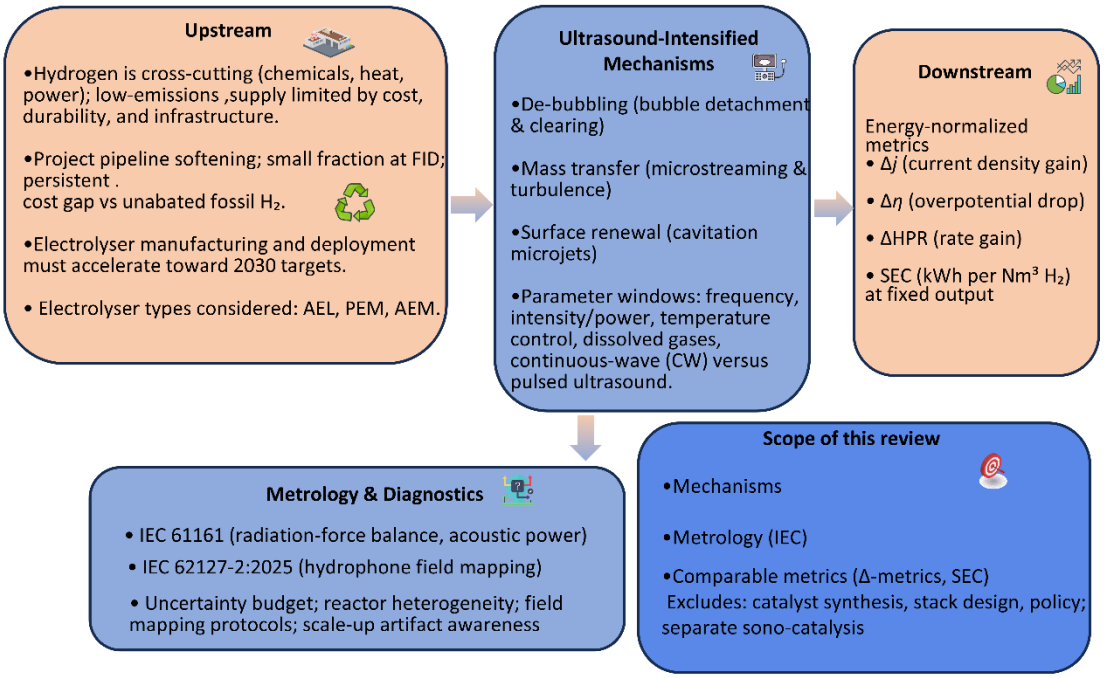

***Figure 1**. Positioning of power ultrasound*

Ultrasound-based hydrogen production

Power ultrasound assists aqueous hydrogen production through two coupled pathways: sono-physical intensification (acoustic streaming/microstreaming, enhanced mass and heat transport, rapid detachment and dispersion of gas bubbles from electrode surfaces) and sono-chemical effects arising from acoustic cavitation (hot-spot radical chemistry, shock waves, microjets). In electrolyzers, these mechanisms can raise instantaneous H_2 generation rates and lower apparent overpotentials, but the net energy balance is highly parameter-window dependent (frequency, pressure/intensity, duty cycle, temperature, dissolved gas, geometry). Reactor-scale studies and reviews consistently caution that gains in rate may coexist with reduced overall efficiency unless acoustic coupling and thermal management are engineered with quantitative cavitation diagnostics and standardized power measurement [4,9-12]. To disentangle transport from collapse-chemistry and set the terminology used below, Figure 2 partitions ultrasound effects into a sono-physical (transport-dominated) branch and a sono-chemical (collapse-chemistry) branch, and summarizes the parameter windows and metrology anchors adopted in this review. Consequently, metrology,

calibrated acoustic power and traceable field mapping must accompany performance claims to enable cross-study comparison [5,6,13,14].

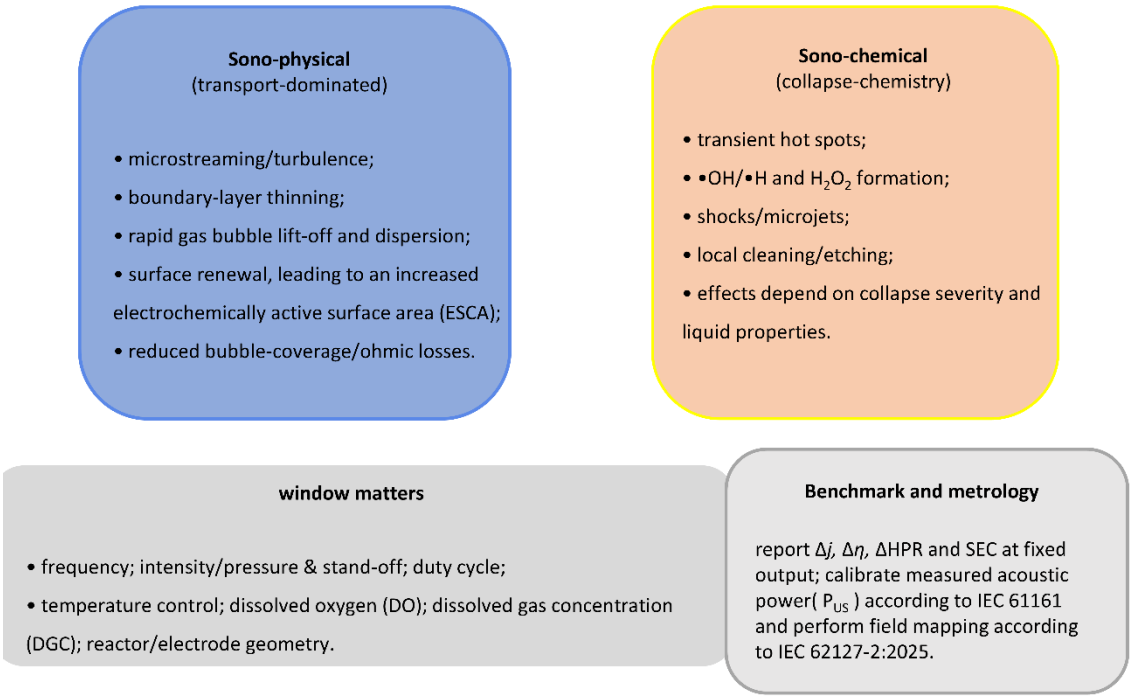

Figure 2. *Sono-physical* vs. *sono-chemical pathways and operating-window variables*

Principles of sonochemistry

Acoustic cavitation, the nucleation, rectified-diffusion growth, and collapse of gas/vapor bubbles, creates transient hot spots (order-of-magnitude $T \sim 10^3$ to 10^4 K, $P \sim 10^2$ MPa) with µs lifetimes, while bubble oscillations and collapses drive vigorous microhydrodynamics that intensify interfacial transport [15,16]. Distinguishing sono-chemical (·OH/·H formation, H_2O_2, radical microchemistry) from sono-physical contributions (boundary-layer thinning, degassing, bubble shedding) is essential for electrode processes: the former scales with collapse severity and liquid properties, whereas the latter reflects streaming and secondary Bjerknes forces in the acoustic field [2,9]. In alkaline and model cells spanning 20 to 600 kHz, controlled studies attribute most HER improvements to bubble-coverage mitigation and surface refresh rather than direct radical participation in charge-transfer steps; tuning frequency and waveform around the electrode zone is therefore critical [12,17]. Since both chemistry and transport depend strongly on the spatial dose of ultrasound, contemporary best practice combines calorimetry and chemical dosimetry (iodide/coumarin assays) with sonochemi-luminescence (SCL) imaging to map active zones and separate chemical from physical effects [18-20]. Large probe-type systems exhibit pronounced geometric dependencies (probe diameter/amplitude, horn immersion, vessel shape), so generator-percentage readouts are not a substitute for acoustic dose [19-21]. For reproducibility, acoustic parameters should be reported with IEC-traceable methods, radiation-force balance for total power (IEC 61161) and hydrophone calibration for field charac-terization (IEC 62127-2:2025), with explicit uncertainty budgets [5,6,13].

Fundamentals of cavitation theory and bubble dynamics

Bubble dynamics are captured by Rayleigh-type formulations for inertial collapse and by Keller-Miksis/Gilmore-type equations for finite-Mach, large-amplitude oscillations; stochastic forcing models approximate noisy drives typical of tanks and flow cells [15,22-24]. These frameworks rationalize threshold behaviour (stable *vs.* transient cavitation), harmonic/subharmonic spectra and

broadband noise, and the conditions for jetting near walls and electrodes, phenomena central to the efficacy of sono-electrolysis and electrode integrity [25].

Cavitation history

The intellectual lineage runs from Rayleigh's spherical cavity collapse [22] to the formal Rayleigh-Plesset class and compressible corrections (Keller-Miksis), with monographs by Brennen [15] and Leighton [16] establishing the scaling arguments that still guide reactor design and diagnostics; Neppiras [26] further codified terminology and experimental caveats foundational to sonochemistry

Cavitation bubble formation and collapse mechanisms

Understanding the formation mechanisms and dynamic behaviours of cavitation bubbles is important for ultrasound-activated processes, including ultrasonic hydrogen generation. The formation of cavitation bubbles involves several stages: nucleation, bubble growth, bubble stabilization and bubble collapse. To visualize the sequence and its implications at electrodes, Figure **3** summarizes the cavitation bubble life-cycle under acoustic drive and contrasts bulk spherical collapses with near-wall asymmetric jetting relevant to bubble shedding and surface renewal.

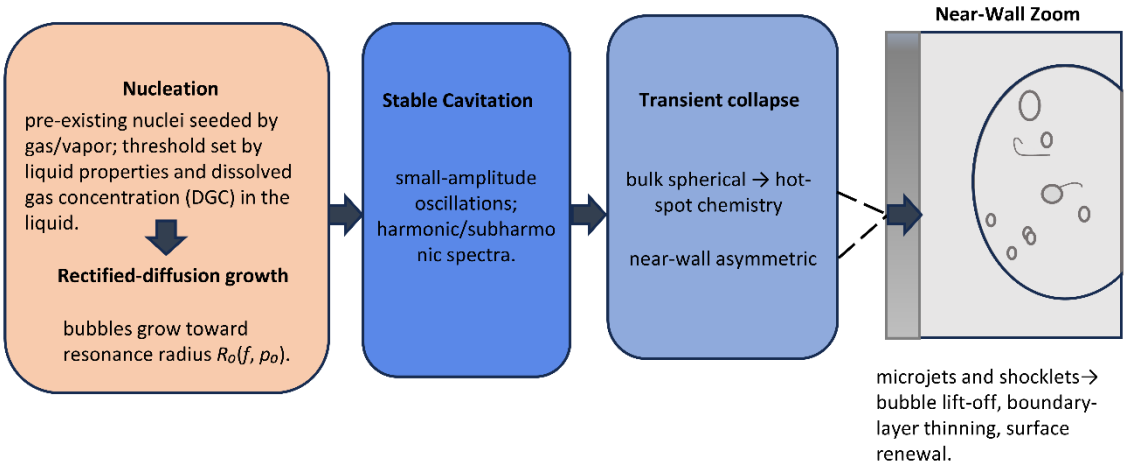

Figure 3. *Cavitation bubble life-cycle and near-wall collapse modes under ultrasound.* f *denotes the ultrasound frequency;* R_o *denotes the ambient bubble radius corresponding to Minnaert resonance at ambient pressure* p_o*. Increasing f leads to a decrease in* R_o*. At high acoustic power, shielding effects and field non-uniformity may become significant, potentially resulting in saturation or reversal of the net effects*

Under acoustic drive, pre-existing nuclei grow by rectified diffusion toward a resonance size set by frequency and ambient pressure; subsequent collapses are nearly spherical in bulk liquids but become strongly aspherical near boundaries [27-29]. Spherical collapses favour hot-spot chemistry, whereas near-wall collapses and bubble-bubble coupling (secondary Bjerknes) promote microjets, shocklets, and vigorous streaming that detach nascent H_2/O_2 bubbles, suppress coalescence, and thin boundary layers, thereby reducing bubble-coverage overpotential and ohmic losses [30-32]. High-speed visualizations and parametric energy analyses in electrolyzers are consistent with bubble-layer thinning and improved gas release under 20 kHz insonation; at higher frequencies (≈200 to 600 kHz), gentler collapses and enhanced rectified diffusion can improve mass transfer at fragile or photoactive interfaces when the acoustic focus coincides with the electrode zone [12,17,33]. Modern variants of classical models extend to finite-Mach oscillations, viscous/non-Newtonian electrolytes, and stochastic fields representative of industrial reactors, predicting frequency-dependent optima and sensitivity to dissolved gas and vapor pressure [24]. Importantly, non-uniform fields and acoustic

shielding at high input power can saturate or reverse gains; hence the need to pair frequency/intensity sweeps with Δ-metrics (Δ*j*, Δ*η*, ΔHPR) and energy-normalized figures (kWh·kg^{-1} H_2) [9].

Detection techniques and *characterization* of acoustic cavitation

(i) Acoustic output and field metrology. Recent work increasingly follows IEC standards. IEC 61161 specifies radiation-force balance (RFB) for total ultrasonic power and associated uncertainty budgets, while IEC 62127-2:2025 provides absolute/relative hydrophone calibration over 50 kHz-100 MHz for traceable field mapping; national metrology labs summarize sensor physics, spatial averaging corrections, and high-intensity considerations [5,6]. Image-guided radiation-force measurements further support calibration and beam characterization under practical reactor conditions [34].

(ii) Passive acoustic monitoring and imaging. Passive cavitation detection (PCD) and passive acoustic mapping (PAM) localize broadband emissions (inertial collapses) and harmonic/subharmonic signatures (stable cavitation); recent implementations provide 2D cavitation maps co-registered with B-mode images, enabling correlation between cavitation activity and bubble shedding in sonicated cells [14].

(iii) Chemical dosimetry and SCL. KI/iodide (I_3^-) and coumarin (7-hydroxycoumarin) assays quantify oxidizing capacity, while SCL visualizes active zones. Multi-factor studies at 20 kHz show strong geometric effects and non-linear dosimetry-SCL correlations, motivating dose-controlled bench-marking rather than single-point snapshots [35].

(iv) Optical/high-speed imaging; scale-aware mapping. High-speed imaging captures plume dynamics, jetting, and vapor clouds; at larger scales, activity meters and dye-degradation surrogates enable reactor mapping to place electrodes in zones of effective cavitation/streaming and to monitor shielding on power ramp-up [10,34]. To align diagnostics with the quantities they constrain and to anchor claims to IEC-traceable metrology, Table 1 summarizes each method versus what it directly or indirectly measures.

Table 1. *Ultrasound cavitation diagnostics and the quantities they measure*

Method	Total acoustic power (IEC 61161)	Acoustic pressure field	Stable	Spatial localization (2D/3D)	Chemistry	Uncertainty
RFB	✓	—	—	—	—	✓
Hydrophone	△	✓	△	✓	—	✓
PCD / PAM	—	—	✓	✓ / △	—	△
SCL	—	—	△	✓	△	△
Chemical dosimetry	—	—	△/—	—	✓	△
High-speed imaging	—	—	△	✓	—	△

Legend: ✓ directly measured; △ indirectly inferred or estimated; — not reported or not applicable. The table summarizes whether each diagnostic method can directly or indirectly quantify the listed quantities under typical experimental conditions.
Notes: Hydrophone-based mapping requires spatial averaging and correction in strong cavitation fields; fibre-optic probes or reduced-power measurements are often employed. PCD typically provides single-element or limited spatial information, while PAM arrays enable two- or three-dimensional localization. SCL and chemical dosimetry indicate chemical activity or hot-spot formation and do not replace acoustic field measurements. All diagnostics should be co-registered with electrochemical measurements; SEC must be reported at fixed output to define system boundaries.

Summary of key literature and milestones in sono-hydrogen research

Table 2 presents a compilation of pivotal cases, spanning from early Sono Hydro Gen experiments to more recent, larger-scale retrofits. Across these studies, frequencies in the 20-200 kHz range, combined with moderate acoustic power densities and controlled temperature, are consistently associated with stronger cavitation activity and improved hydrogen production metrics.

***Table 2**. A whole summary of recent studies*

Frequency, kHz	Liquid temperature, °C	Output, power, W	Acoustic intensity, W·cm^{-2}	Reactor size, ml	Result
20 200 500 800	20	30	-	300	The production rate of hydrogen peroxide (H_2O_2) was measured at 0.7 µmol·min^{-1} under 20 kHz sonication, escalating to 5 µmol·min^{-1} at 200 kHz [36] .
20 200 500 800	40	30	-	250	The molar production rate of hydrogen peroxide (H_2O_2), was documented as 1.1 µmol·min^{-1}, at 20 kHz ultrasonic excitation and escalated to 5.2 µmol·min^{-1}, under 200 kHz operation [37]
213 to 1100	-	-	1	-	The rate of generation of H_2O_2 is 2.1 µmol·min^{-1}at 1140 kHz and 4.2 µmol·min^{-1} at 585 kHz [38]
20	30	-	26	-	[39]
200	5-50	-	6	38	[40]
42	22-25	100	-	300	[41]
20	-	-	-	1000	Experimental results indicated a 4.5 % gain in production throughput and a 1.3 pp (percentage point) elevation in energy conversion efficiency under ultrasonic excitation [42]
40	-	60	-	300	After integrating ultrasonic treatment into the electrolysis process, the hydrogen yield increased by an average of 3.93 % [43]
381 863 992 1176	20	250	-	40-700	[44]
20 100 362	18	-	-	250	[45]
20	25	10 to 40	-	250	[46]
40	25 to 45	-	38	20	[47]
300	20	77.2	-	220	The hydrogen yield rate increases with the concentration of the specific alcohol; it reaches the maximum value (5.46 µmol·min^{-1}) at 5 % methanol concentration [48].
40	27, 40, 45, 50, 55 and 60	60	-	300-350	Ultrasonic treatment significantly improved hydrogen production efficiency and reaction kinetics, especially in continuous mode [49]

Taken together, Table 2 highlights how frequency, acoustic intensity and temperature jointly shape hydrogen yield across diverse systems. Building on this compilation, section *Parameters affecting performance* analyses these parameters in detail, linking operating windows to underlying cavitation and transport mechanisms.

Parameters affecting performance

The efficiency and selectivity of ultrasound-assisted water electrolysis (sono-electrolysis) are governed by a coupled set of acoustic-electrochemical variables. Among these, frequency, acoustic intensity, and temperature determine bubble dynamics, mass/charge transfer and interfacial kinetics; waveform (CW vs. pulsed) and dissolved-gas composition further modulate cavitation activity, bubble residence, and the boundary-layer thickness adjacent to electrodes. A parameter window that boosts H_2 production rate without degrading specific energy consumption (SEC) is therefore essential to evaluate “true” gains beyond apparent rate increases [50-52].

Cavitation phenomena vary markedly across operating conditions, and recent experiments have begun to map these dependencies, although several parameters remain to be systematically explored. To orient subsequent sections, Table 3 summarizes the operating windows that link frequency, acoustic intensity and temperature to dominant phenomena and electrode suitability.

***Table 3**. Operating windows: frequency × intensity × temperature. Representative sources: [28,51,53-56]*

Frequency band, kHz	Low intensity	Mid intensity
20 to 40	Detachment-dominant; strong acoustic streaming; suited to smooth/planar Ni	Transient cavitation; rapid gas clearing; monitor heating/thermal drift
200 to 600	Stable cavitation; fine-scale streaming; suited to porous/DHBT Ni	Rectified diffusion increases; de-gassing of pores; gentler on surfaces

Note. Operating windows are geometry-dependent and couple frequency, delivered intensity at the electrode, and temperature to dominant phenomena and electrode suitability. Run isothermally (20 to 35 °C) and report geometry/stand-off and runtime. Intensity refers to delivered dose (not electrical input); measure acoustic power/field with IEC 61161 (RFB) and IEC 62127-2:2025 (hydrophone), including uncertainty.

Table 3 thus provides the operating map: sections *Frequency: From transient cavitation to gentle streaming, Acoustic intensity, Temperature* and *Interactions among frequency, intensity, and temperature* discuss the underlying physics along each axis, and sections *Acoustic waveform: Continuous vs. pulsed ultrasound*, *Dissolved gas content: An important control variable* and *Performance benchmarks and common failure modes* translate this into framing, evidence, design rules and reporting guidance.

Frequency: from transient cavitation to gentle streaming

Low frequencies (18 to 40 kHz) foster transient cavitation, vigorous microstreaming, and strong primary/secondary Bjerknes forces. These effects efficiently shed hydrogen bubbles from the cathode, thin the gas blanket, and reduce bubble overpotential, particularly on textured Ni or DHBT-porous Ni surfaces. High frequencies (200 to 600 kHz) suppress violent collapses but promote stable cavitation and fine-scale acoustic streaming that de-gas the diffusion layer without excessive erosion of catalyst surfaces. Comparative experiments on planar vs. porous Ni under 20 kHz vs. ~580 kHz fields show that both regimes reduce HER overpotential, but the optimum frequency depends on porosity, stand-off distance, and bath geometry; porous Ni tends to benefit at both bands provided the acoustic path is well-coupled [3,12,17].

Three practical points emerge:

No universal "best" frequency. On smooth plates at modest current densities, 20-40 kHz often maximizes detachment; with meso/macro-porous Ni, 200 to 600 kHz can outperform by sweeping bubbles out of cavities without re-entrainment [12].

Volumetric resonance matters. At near bubble resonance, rectified diffusion and streaming spike, amplifying mass transfer; off-resonance operation blunts benefits [43].

Document the geometry. Electrode-to-sonotrode distance (and angle) strongly modulates delivered intensity at the electrode. Report frequency, nominal power, distance, and coupling medium to ensure reproducibility [57].

Existing studies suggest that "optimal" frequency is system-dependent rather than universal. In practice, frequency should be considered together with delivered acoustic intensity, temperature and cell geometry. Further parametric studies that vary these factors jointly would help to identify practical operating windows for different electrode architectures and electrolyser designs.

Acoustic intensity

Most power values in sono-electrolysis are electrical inputs to the transducer, not the delivered acoustic dose at the electrode. Where possible, quantify the field using hydrophone calibration or calorimetry and report $W \cdot cm^{-2}$ (or MPa peak negative pressure). As a rule of thumb, 0.2 to 1.0 $W \cdot cm^{-2}$ at 20 to 40 kHz is sufficient to dislodge adherent H_2 bubbles and lower the cell voltage by 0.2 to 0.6 V at fixed current in small cells; higher intensities bring diminishing returns and more heating. Recent catalyst-agnostic studies further confirm that ultrasound reduces bubble residence

time up to ~80 %, regenerates active surface, and sustains Ni catalysts by periodic micro-cleaning [57]. To avoid conflating electrical drive with acoustic dose, we plot delivered acoustic intensity at the electrode (W·cm^{-2}) against a normalized bubble burden (B/B_0), where B/B_0 is computed from surface coverage, gas-layer thickness δ or bubble residence time (t_{res}) as B/B_0 ={coverage/coverage$_0$, δ/δ_0, $t_{res}/t_{res,0}$}. Here, coverage$_0$, δ_0 and $t_{res,0}$ denote the corresponding baseline values measured under silent (no-ultrasound) operation at the same current density, bulk temperature and geometry. As shown in Figure 4, within the commonly used 20 to 40 kHz window, there is an illustrative effective band in which increasing delivered intensity from sub-watt levels up to about 1.0 W·cm^{-2} rapidly reduces B/B_0 (detachment/streaming-dominated thinning). Beyond this range, diminishing returns appear and a high-intensity caution zone emerges where cavitation-cloud shielding and local heating can offset or even reverse gains. Two x-anchors at 0.177 and 0.253 W·cm^{-2} come from hydrophone/RFB-calibrated 40 kHz measurements; studies that did not report delivered intensity are placed qualitatively along the band using their B/B_0 values. Delivered intensity and its uncertainty should be reported with IEC 61161 (acoustic power) and IEC 62127-2:2025 (hydrophone field mapping), and high-drive artefacts confirmed with PCD/PAM and SCL alongside bath-temperature logging.

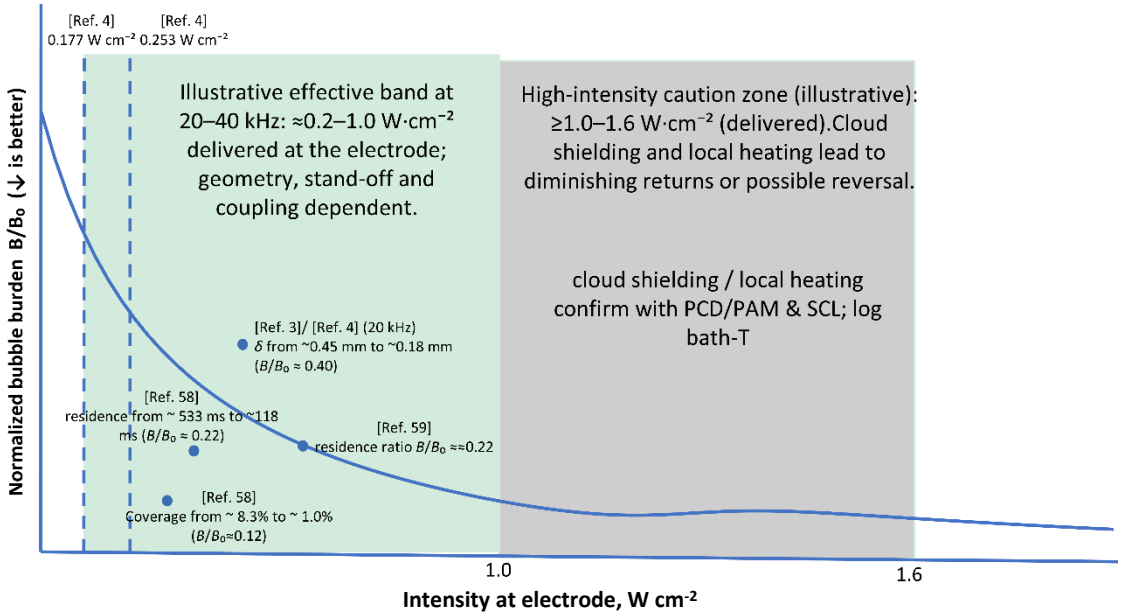

Figure 4. *Delivered acoustic intensity at the electrode versus normalized bubble burden (B/B_0) Data points are adapted from representative studies [3,4,58,59]. Note: The trend is illustrative (not to scale); unlabelled x-positions are qualitative, and standards IEC 61161 and IEC 62127-2:2025 are recommended for reporting delivered intensity with uncertainty*

A rapid decline of B/B_0 is observed in an illustrative, geometry-dependent band at 20 to 40 kHz (≈0.2 to 1.0 W·cm^{-2}), followed by diminishing returns as cloud shielding and local heating arise (grey caution zone, ≥1.0 to 1.6 W·cm^{-2}). Vertical dashed lines at 0.177 and 0.253 W·cm^{-2} are calibrated x-anchors. Representative y-values positioned qualitatively within the band denote literature-reported ranges compiled across multiple studies, rather than time-resolved trajectories. Within this window, surface coverage decreases from ~8.3 to ~1.0 % (B/B_0 ≈ 0.12), bubble residence time decreases from ~533 to ~118 ms (B/B_0 ≈ 0.22), and the estimated gas-layer thickness δ decreases from ~0.45 to ~0.18 mm (B/B_0 ≈ 0.40), and a PEM case with $t_{res}/t_{res,0}$ ≈ 0.22. All values are reported in terms of delivered acoustic intensity at the electrode, measured or inferred using IEC-traceable methods, with associated uncertainties.

The left-hand trend consolidates multi-study evidence that ultrasound primarily improves HER via bubble-coverage mitigation and boundary-layer thinning, which manifest as $B/B_0 \approx 0.12$ to 0.45 across different cells and electrodes at low-mid drive; corresponding cell-voltage drops originate from reduced bubble and ohmic losses. The right-hand caution zone reflects physics rather than noise: cavitation-clouds can attenuate incident acoustic energy to a small, transmitted fraction and high drive elevates bulk and near-electrode temperatures - both mechanisms explain the flattening/possible reversal of benefit. For reproducibility and comparability, experiments should specify frequency, waveform/duty, delivered intensity at the electrode, stand-off and geometry, electrolyte and dissolved-gas conditions, temperature control, and corroborate field/dose with IEC-traceable metrology.

Building on Figure 4, in which delivered acoustic intensity at the electrode was identified as the primary lever for bubble removal within an illustrative 20-40 kHz band, we next examine how frequency modulates performance at practical intensities (≤ 1.0 W·cm^{-2}). To avoid overdriving and thermal artefacts, the datasets discussed here are delivered at intensities between 0.0 and 1.0 W·cm^{-2} (unless stated otherwise), and intensities refer to the acoustic dose at the electrode rather than the electrical input power.

Additionally, complementing the experiments, Kerboua and Hamdaoui [60] numerically estimated H_2 generation under varied acoustic pressure amplitudes and frequencies. As summarized in

Table **4**, raising acoustic amplitude increases the predicted H_2 production rate at both 200 kHz and 1 MHz, whereas higher frequencies substantially suppress absolute yields at the same amplitude. Although model-dependent, these results corroborate the experimental trend that intensity increases are beneficial within the sub-W to ~1 W·cm^{-2} window, while frequency tunes cavitation severity and transport pathways.

***Table 4**. H_2 production (mol) at different acoustic power and frequencies [60]*

	Acoustic pressure amplitude, kPa			
	152.0	202.7	253.3	304.0
Acoustic frequency	H_2 production, mol			
200 kHz	1.3×10^{-19}	2.53×10^{-17}	7.35×10^{-17}	1.30×10^{-16}
1000 kHz	2.95×10^{-33}	5.67×10^{-24}	1.64×10^{-21}	2.91×10^{-19}

Taken together, the literature supports a window-based operating strategy: keep the delivered intensity in the 0.2 to 1.0 W·cm^{-2} range to harvest detachment- and streaming-driven gains and use frequency to match the electrode/geometry (*e.g.* 20 to 40 kHz for aggressive de-bubbling on smooth plates; 200 to 600 kHz for gentler de-gassing of porous structures). Beyond ~1.0 to 1.6 W·cm^{-2}, cloud shielding and local heating can flatten or negate benefits; therefore, intensity-frequency sweeps should be paired with SEC and Δ-metrics (Δj, $\Delta\eta$, ΔHPR) under isothermal control. For comparability, report the delivered dose using IEC 61161 (acoustic power) and IEC 62127-2:2025 (hydrophone field mapping), including the geometry and standoff and the associated uncertainty budgets. This framing recasts frequency versus intensity as a tractable design problem and avoids single-point claims that conflate electrical input with acoustic exposure.

Temperature

Temperature co-determines both kinetic constants (Arrhenius) and two-phase transport (gas solubility, viscosity, surface tension). In silent AWE, raising the temperature generally improves kinetics and conductivity. Under ultrasound, the sign can invert if warmer electrolytes diminish the acoustic contrast, driving bubble removal.

Low temperature (10 to 25 °C)

At low temperatures, gas solubility is higher and viscosity is larger; bubbles detach less readily in silent cells. Here, ultrasound is disproportionately beneficial: on Raney-Ni at 408 kHz, ~25 °C, ultrasound boosts HER more than at elevated temperature, consistent with stronger relative gains when bubble adhesion is worst [17].

Elevated temperature (40 to 60 °C)

With rising temperature, silent-cell performance already improves, and the incremental ultrasound benefit can shrink. Overheating the bath during ultrasonication (poor thermal management) further reduces cavitation intensity. Maintain isothermal control and report bulk temperature and run time; decouple thermal from acoustic effects [3].

Here, we decouple thermal gains from acoustic gains. Figure 5 contrasts the silent-cell baseline with the ultrasound-induced increment as a function of temperature, using dimensionless, normalized axes.

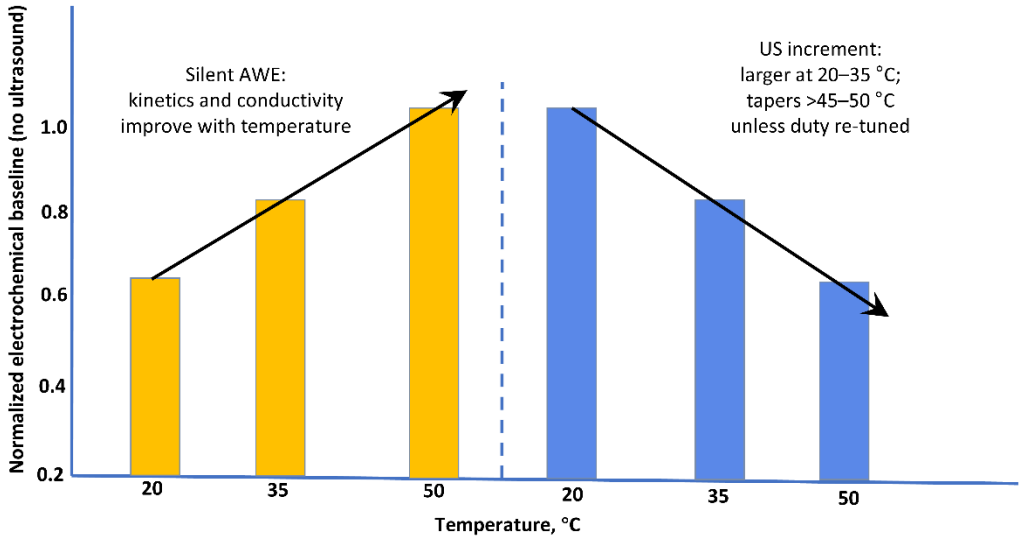

Figure 5. *Temperature effects: silent baseline versus incremental ultrasound benefit (schematic). Temperature refers to the bulk electrolyte temperature, °C. Maintain an isothermal clamp; report bulk* T *and run time. Higher* T *increases vapor content and cushions collapses, leading to weaker cavitation benefit. For delivered dose reporting, follow IEC 61161 (acoustic power) and IEC 62127-2:2025 (hydrophone).*

The left panel shows that the silent alkaline water electrolysis (AWE) baseline improves with temperature (faster kinetics, higher conductivity). The right panel isolates the ultrasound increment at the same temperature, largest around 20 to 35 °C and tapering above ~45 to 50 °C unless duty/ /coupling are re-tuned, consistent with increased vapor content and cushioned collapses at higher temperature [61,62]. To ensure comparability with the intensity windows in Figure 4 and the operating map in Table 3, all temperatures are run isothermally, bulk temperature and runtime are reported, and "intensity" elsewhere refers to delivered dose at the electrode (IEC 61161/IEC 62127-2:2025). This framing prevents conflating simple heating with true cavitation-mediated benefits and clarifies why tuning duty/stand-off is often required at elevated temperature.

In alkaline AWE, the silent baseline improves with temperature because charge-transfer kinetics accelerate and electrolyte conductivity increases. By contrast, the incremental benefit of ultrasound declines as temperature rises. For example, at 408 kHz on Raney-Ni, the enhancement observed at 25 °C is markedly reduced at 40 to 60 °C, even though the silent baseline improves, providing direct evidence that the ultrasound increment weakens at higher temperatures [17]. This behaviour is

consistent with higher vapor pressure and dissolved-gas content at elevated *T*, which cushion bubble collapses and shift cavitation from transient to gentler regimes [62]. For comparability, experiments should be conducted isothermally at the bulk temperature, with runtime logged, and intensities reported as delivered at the electrode using IEC-traceable methods (IEC 61161 for acoustic power; IEC 62127-2:2025 for hydrophone-based field mapping). As temperature rises, the baseline improves, whereas the ultrasound increment often contracts because the effective intensity window shifts; sustaining a positive increment at elevated temperature usually requires retuning duty and stand-off.

Interactions among frequency, intensity, and temperature

The three parameters interact non-linearly through two channels: (i) bubble dynamics (nucleation, growth, coalescence, detachment) and (ii) near-wall flow (streaming that thins concentration/thermal boundary layers). Empirically:

20 to 40 kHz, 0.2 to 1.0 W·cm^{-2}, 20 to 35 °C often maximizes detachment-limited HER on smooth Ni or stainless steel, especially at high current density [3,12,43].

200 to 600 kHz, 0.05 to 0.3 W·cm^{-2}, 20 to 35 °C is attractive for porous electrodes, minimizing re-entrainment while preserving structure [12,43].

Above ~45 to 50 °C, ultrasound gains on HER taper unless geometry or waveform is re-optimized (*e.g.* duty-cycled bursts to curb heating) [3,12,43].

Overall, the interactions between frequency, delivered acoustic intensity and temperature control cavitation behaviour and the local electrochemical environment, and hence the achievable hydrogen production rate. Multi-parameter coupling models that treat these variables jointly would be useful for designing operating windows with favourable trade-offs between production rate and specific energy consumption. The next section, therefore, examines how the acoustic waveform (continuous versus pulsed) further modulates cavitation structure and hydrogen production efficiency.

Acoustic waveform: Continuous vs. pulsed ultrasound

Building on the operating windows (frequency-intensity-temperature), the waveform is a time-domain control knob at fixed delivered dose: CW sustains steady streaming and continuous bubble sweeping, whereas PU redistributes dose into on-off bursts to limit heat load while preserving detachment cycles.

In side-by-side tests on membraneless alkaline cells, CW reduced bubble-related resistance more (≈ -76 %) than untuned pulsed mode at equal average input, but optimized duty cycles narrowed the gap while reducing temperature rise; on/off control at 20 kHz improved power efficiency when the “on” phase targets detachment and the “off” phase avoids over-mixing [59].

Comparative experiments further show that PU can shrink bubble size (≈17 μm), reduce residence time (~80 %), and increase current density (~9 %) in alkaline electrolysis [58,63-66], and that the benefit depends on pulse length/interval rather than being universally superior to CW [67].

On this basis, practical design rules include the following:

- Prefer CW for short, low-temperature runs where maximum continuous sweeping is required and heating is not limiting.
- Prefer PU for long runs or elevated *T*, or when cloud shielding/overheating push operation beyond the effective band (link to Figure 4). Start with duty 10 to 30 %, PRF 100 to 1000 Hz, burst 1 to 5 ms, then refine experimentally.
- Keep delivered intensity at the electrode within the Figure 4 window; at *T* >45 to 50 °C (Figure 5) expect the US increment to taper and re-tune duty/stand-off accordingly.

- Always interpret waveform effects in the context of geometry and coupling.

For waveform studies, reports should at a minimum specify the applied frequency and full pulse descriptor (duty cycle, PRF and burst length), together with bulk *T* and runtime, and should present performance as Δ-metrics and SEC. The remaining acoustic and electrochemical metadata can follow the minimum reporting set outlined in section *Performance benchmarks and common failure modes.*

Dissolved gas content: An important control variable

Dissolved-gas concentration/composition (DGC) sets cavitation inception, bubble life and sonochemistry; it must be controlled when comparing frequency or duty sweeps.

Theory and experiments show that higher DGC lowers inception thresholds and promotes rectified diffusion; gas identity (Ar, air, N_2, CO_2) shifts radical yields and cavitation behaviour across 20 to 300 kHz sonoreactors, translating into different detachment/coalescence patterns at otherwise identical acoustic settings [68,69]. Continuous DO monitoring reveals dynamic depletion/re-equilibration during insonation; CO_2 and high-DGC conditions can alter cavitation chemistry and wetting [70] and, at high drive, foster coalescence/cloud shielding [68,71]. Broader reviews and recent studies quantify typical Ar > air > N_2 ≫ CO_2 trends in radical yield/sonoluminescence and analyse DGC-dependent bubble dynamics [71-73]; parametric work further links DGC to stable bubble size/life [74].

Based on these observations, practical design rules include the following:

- Fix gas identity and target DO/DGC before sweeps; re-equilibrate between runs and log DO *vs.* time.
- Use Ar/air when probing sono-chemical leverage; use N_2 to isolate sono-physical effects (streaming/detachment) with minimal radical chemistry.
- At high DGC or high drive, anticipate coalescence/shielding and confirm with PCD/PAM/SCL diagnostics where available [75-77].
- Co-design DGC with temperature and waveform to stay inside the effective window.

For reporting, experimental studies should specify gas identity, DO/DGC (initial value, trajectory, conditioning protocol), electrolyte pH/conductivity drift, and geometry/stand-off; compare at equal delivered intensity and bulk temperature; co-register diagnostics with electrochemistry (*V*-*j*-*T*-HPR) where *V* is the cell voltage, *j* the current density, *T* the bulk temperature, and HPR the hydrogen production rate (gain reported as ΔHPR). follow IEC 61161/IEC 62127-2:2025, specifically the section "Detection techniques and characterization of acoustic cavitation."

Table 5 aligns dissolved-gas identity/level with cavitation fingerprints and reporting requirements, standardizing DO/DGC control across frequency/duty sweeps and making results comparable across labs. The standards and diagnostics context follow IEC 61161/IEC 62127-2:2025, specifically the section "Detection techniques and characterization of acoustic cavitation."

Table 5. *Gas/DGC cavitation fingerprints and reporting requirements*

Gas/DGC	Inception threshold	Radical yield tendency	Bubble life and detachment	Electrolysis-specific notes	Reporting
Ar (moderate DGC)	Low-to-moderate at matched DGC; promotes transient cavitation [73]	High (higher hot-spot temperature; strongest SL/H_2O_2 yields) [73]	Shorter bubble life; strong microjets facilitate efficient detachment [73]	Good de-bubbling; at high drive watch erosion/pitting on Ni	log DO *vs.* time; state gas mixture; compare at equal delivered intensity and bulk temperature
Air (ambient DGC)	Moderate [73]	Moderate [72]	Balanced detachment/coalescence [72]	Convenient baseline; composition drifts under insonation (O_2 depletion) [68]	log DO; re-equilibrate between runs; control headspace[68]

Gas/DGC	Inception threshold	Radical yield tendency	Bubble life and detachment	Electrolysis-specific notes	Reporting
N_2 (moderate DGC)	Slightly higher than Ar at matched DGC [73]	Lower (quencher; radical yields suppressed) [73]	Longer bubble life; slower detachment (predominantly sonophysical) [73]	Useful to isolate streaming/detachment without strong sonochemistry	Report DO target and equilibration protocol; compare at same *j*, *T* and delivered dose
CO_2 (controlled DGC)	Easy inception; nuclei abundant [73]	Mixed/low; pH shift alters metrics and speciation [68]	Fine bubbles; altered coalescence patterns; wetting modified [68]	Carbonate formation in alkaline media; conductivity & pH drift [68]	Report pH drift; justify use-case; maintain isothermal control; log DO trajectory
DGC increases (general)	Threshold decreases (lower nucleation barrier) [73]	- (identity-dependent)	Coalescence or cloud shielding increases at high drive leads to attenuation and non-uniform fields [78-80]	May flip net benefit without thermal/field control	State limits for DO/DGC; confirm field with PCD/PAM/SCL; co-register with *V-j-T*-HPR [75-77]

Note: Trends are geometry- and frequency-dependent. Control gas identity and DO/DGC when comparing frequency or duty; co-register diagnostics with electrochemistry; report delivered intensity at the electrode and bulk temperature (IEC 61161/IEC 62127-2:2025).

Performance benchmarks and common failure modes

Across electrodes and cell formats, replicable ultrasound benefits cluster around thinner gas layers, shorter residence/smaller departure, and lower cell voltage/SEC, provided the acoustic window is tuned and thermal drift is controlled.

Well-reported studies converge on the following trends:

(i) δ shrinking from ≈0.45 to ≈0.18 mm with V_{cell} drops ≈0.3 to 0.6 V at fixed j in small AWE cells [3].

(ii) residence-time reduction up to ~80 % with smaller departure sizes and lower bubble overpotential [52].

(iii) net energy-efficiency gains of ~10 to 25 % when the delivered dose is tuned and runs are isothermal [12,54].

Frequent pitfalls include unreported geometry/stand-off, absence of hydrophone/calorimetry, bath-temperature drift, and changing DO/DGC, all capable of flipping the sign of the "ultrasound benefit" [68]. Where available, PCD/PAM and SCL/chemical dosimetry provide corroborating field maps to de-bias single-point snapshots.

Corresponding design rules are to evaluate and report Δ-metrics (Δj, Δη, ΔV_{cell}, ΔHPR) and SEC at a fixed output, and to keep operation within the delivered-intensity window (Figure 4) while retuning at elevated temperature (Figure 5). Above ~1 W·cm^{-2}, cloud shielding/heating may cause diminishing returns; verify with PAM/PCD/SCL and bath-temperature logs.

The minimum metadata set for sono-electrolysis studies should include: frequency; a full waveform description (duty/PRF/burst); delivered acoustic intensity at the electrode (W·cm^{-2} or peak negative pressure); stand-off/angle, electrode morphology, electrolyte composition and conductivity; bulk temperature and runtime; DO/DGC. Acoustic power (IEC 61161) and field distributions (IEC 62127-2:2025) should be calibrated with stated uncertainty budgets.

In summary, performance in ultrasound-assisted water electrolysis is window-dependent, governed jointly by frequency, delivered intensity at the electrode, temperature, waveform, and dissolved-gas content. Low-frequency fields tend to favour transient cavitation and bubble detachment, whereas higher frequencies promote stable cavitation and fine streaming, benefits that shift with geometry and stand-off, so no universal optimum exists. Pulsed operation can preserve detachment cycles while limiting heating when duty/PRF are tuned; at elevated temperature, the ultrasound increment often tapers and requires re-tuning. For comparability, outcomes should be reported as Δ-metrics (Δj, Δη, ΔV_{cell}, ΔHPR) and SEC under isothermal control, with acoustic power/field measured using IEC-traceable methods. This window-aware, metrology-

anchored view sets up section *Hybrid sono-hydrogen systems*, where we formalize reporting structures, uncertainty budgets and multi-field coupling strategies.

Hybrid sono-hydrogen systems

Introduction to multiphysics coupling in hydrogen production

Coupling power ultrasound (US) with electric (E), thermal (T) and magnetic (M) fields disturbs interfacial gas management and ionic/molecular transport in ways that conventional electrolysis cannot. Properly tuned, ultrasound thins gas films, accelerates bubble detachment, and enhances near-electrode convection; conversely, it can add parasitic energy and thermal loads if not metrologically constrained. We adopt Δ-metrics - Δj (current density gain at fixed potential), Δη (overpotential reduction at fixed j), ΔHPR (hydrogen production rate gain), and SEC (kWh·kg^{-1} H_2), with SEC including acoustic/auxiliary inputs. This aligns lab claims with DOE/IEA energy accounting and deployment realities [81].

Sections *US-electric coupling systems, US-thermal coupling systems* and *US-magnetic coupling systems* dissect single-field couplings (US-E/US-T/US-M). Section *Multi field hybrid systems coupling* synthesizes multi-field stacks (E-M-US-T) with evidence matrices and baseline comparators. section *Cross-coupling metrology and energy accounting* provides the metrology & reporting framework that underpins fair comparisons.

Cross-coupling metrology and energy accounting

To enable apples-to-apples evaluation across laboratories and electrolyser types (AEL/PEM/AEM), we recommend a minimum report set:

(i) IEC-traceable acoustics. Report ultrasonic power P_{US} by radiation force balance (RFB) per IEC 61161 [6]; map acoustic fields with calibrated hydrophones per IEC 62127-2:2025 [5], including bandwidth, complex sensitivity, effective radius, and uncertainty budget. Provide hydrophone calibration traceability to a national metrology institute (*e.g.* NPL/PTB) [57,82,83].

(ii) Energy accounting and Δ-metrics. Accompany Δj/Δη/ΔHPR with SEC (kWh·kg^{-1} H_2) that explicitly includes acoustic, thermal, magnetic, pumping and control loads; specify system boundaries per DOE Hydrogen Shot assessment and IEA Global Hydrogen Review [1,81].

(iii) Operating maps and negative data. Use response-surface designs spanning frequency (20 to 800 kHz), amplitude, duty cycle, electrolyte temperature, and pressure; publish neutral/negative regions to avoid publication bias. Include waveform metadata (CW vs pulsed, burst length, PRF) [12,84-86].

(iv) Co-registered diagnostics. Combine passive acoustic mapping (PAM/PCM) or time-domain PADAM/DMAS with high-speed/ultrafast optical imaging to distinguish stable vs inertial cavitation and to co-localize activity with electrochemical readouts [75,77,87-90].

(v) Thermal management disclosure. Report bulk and interfacial temperatures, heat sinks, and ultrasound-induced heating, noting that elevated temperature weakens collapse intensity and alters mass transfer [91].

US-electric coupling systems

Mechanistic windows and limits

Under US-E, Bjerknes-driven bubble migration, acoustic microstreaming and cavitation-induced roughening act together to (i) clear active sites, (ii) compress diffusion layers and (iii) reduce ohmic film resistance. Net performance gains have been documented from laboratory H-cells to

membrane-free alkaline cells. However, these gains are strongly window-dependent: frequency, duty cycle and temperature jointly determine whether ultrasound reduces overpotential and increases current density (Δj, $\Delta\eta$) or whether additional acoustic power and heating worsen the specific energy consumption (SEC).

A 2024-2025 wave of sono-electrolysis studies, therefore, begins to map "positive" windows—where US yields net $\Delta j/\Delta\eta$ improvements at acceptable SEC, from "negative" windows where bubble shielding, viscous losses and thermal penalties offset any transport benefits [11,12,43,54].

Membraneless and PV-supplied sono-electrolysis

Merabet and Kerboua [11,43,49] coupled a PV-supplied membrane-free alkaline electrolyser with indirect sonication, modelling the bubble coverage fraction on the electrodes and validating their model under real meteorological conditions. They reported reversible ohmic and cell-voltage recovery upon ultrasound application, along with smoother dynamic tracking of intermittent PV power—an archetype for systems-level US-E integration.

In such membrane-free architectures, ultrasound primarily controls bubble accumulation and cross-sectional blockage in shared gas-liquid channels, while its influence on gas purity and crossover becomes critical at higher current densities [49,56].

Pulsed operation and fair electrical baselines

High-frequency pulsed electrolysis (without ultrasound) can mimic some "US-like" benefits by modulating gas production in time and allowing bubbles to detach during the off-periods [84]. However, a recent 2025 analysis finds that, once total charge passed and stack design are kept constant, steady DC operation often minimises SEC, and many reported pulsed protocols improve instantaneous current at the expense of overall energy efficiency [86].

For US-E studies, this implies that claimed ultrasound benefits should be benchmarked not only against a simple DC reference, but also against the best-performing non-acoustic electrical strategies (optimised pulsed and DC conditions) [84,86]

Design guidance for US-E stacks

For planar electrodes at $j \geq 500$ mA·cm^{-2}, recent alkaline sono-electrolysis work suggests that ultrasound in the 20 to 80 kHz range with low duty cycles is particularly effective at detaching millimetre-scale bubbles and suppressing gas films on the electrode surface [50,52,54,56]. At higher frequencies, microstreaming and radiation forces acting on smaller bubbles tend to dominate the enhancement mechanism [17,28,54].

To make such design choices reproducible, researchers should publish P_{US} (measured via IEC-compliant acoustic power methods), acoustic field maps, Δ-metrics (Δj, $\Delta\eta$, ΔHPR) and SEC in line with the reporting framework in section *Cross-coupling metrology and energy accounting* [91]. This helps ensure that reported US-E gains are interpreted as genuine transport and kinetic improvements rather than artefacts of unmeasured acoustic power or uncontrolled heating.

US-thermal coupling systems

Separating genuine cavitation effects from heat

High-intensity ultrasound (HIUS) inevitably deposits heat in the electrolyte and cell hardware. Calorimetric audits and practical heat-management guidelines show that a sizeable fraction of P_{US} can appear as bulk temperature rise unless active cooling and thermal sinks are engineered [85]. Under such conditions, apparent improvements in current density, overpotential, or H_2 production

rate may simply reflect Arrhenius-type electrochemical acceleration and reduced ohmic resistance rather than cavitation-specific transport enhancement. Single-bubble and cloud-dynamics studies further indicate that increasing bulk temperature raises vapour pressure and modifies dissolved-gas content, which shortens collapse duration and lowers peak pressures, thereby weakening inertial cavitation and microjet intensity [91].

Accordingly, US-T studies must include isothermal, non-ultrasonic baselines and in situ thermometry near the electrodes before attributing any Δj, $\Delta\eta$ or ΔHPR to cavitation rather than heat.

Process windows and pitfalls

From an electrochemical standpoint, raising the electrolyte temperature into the 50 to70 °C window typically lowers cell voltage and accelerates charge-transfer kinetics in alkaline water electrolysis, even without ultrasound [61]. When ultrasound is superimposed on this thermally activated regime, the marginal US increment in Δj or $\Delta\eta$ often shrinks and can even reverse once weakened cavitation and increased viscous losses offset the transport gains [85,91]. Temperature also modifies jetting and streaming structures near solid walls, shifting the optimum frequency, duty cycle, and stand-off distance for US-E synergy. To make this interplay transparent, US-T work should report temperature-dependent response surfaces, for example, current density, overpotential, and SEC as functions of (T, P_{US}, frequency, duty cycle), and explicitly identify regimes where ultrasound primarily acts as a heater. In such regimes, performance gains should be attributed to deliberate temperature control, with ultrasound reported as the heating method rather than as a purely "non-thermal" intensification route [85].

In practice, this means that US-T optimisation should start from a well-characterised thermal baseline, and only then ask whether cavitation-driven transport offers any additional benefit.

US-magnetic coupling systems

Under US-M, magnetic fields are used alongside ultrasound to manipulate bubble plumes and electrolyte flow without relying solely on buoyancy. Recent microgravity and terrestrial studies highlight two distinct roles for magnetism: magnetically driven convection as a flow-control tool, and more subtle modifications of electrocatalytic mass transport and current distribution.

Magnetic convection as a flow-control lever

Akay *et al.* [92,93] recently demonstrated in microgravity that a static permanent magnet can induce magnetically driven convection, which enhances electrolysis current densities by up to ~240 % and enables passive gas-liquid separation, even in the absence of buoyancy-driven natural convection. This magnetically induced convection acts as a body force on the paramagnetic electrolyte and on evolving gas bubbles, reorienting flow and bubble trajectories independently of gravity [92]. The same principle is directly transferable to bubble management under terrestrial conditions where buoyancy is weak or geometrically constrained, such as in vertical flow fields, narrow channels, or zero-gap cell architectures [92,93]. In US-M configurations, magnetic convection can therefore be viewed as a complementary flow-control lever that redistributes the bubbles detached by ultrasound, potentially reducing bubble residence times in regions that are otherwise poorly drained.

Magnetic fields and electrocatalysis under US-M

Beyond bubble management, magnetic fields can alter mass transport, current distribution and local overpotentials in electrocatalytic systems through magnetohydrodynamic effects and field-induced changes in concentration gradients [94]. However, most reported performance gains arise

from modified transport rather than intrinsic changes in reaction kinetics, and any comparison between magnetic and non-magnetic operation must be normalised to the auxiliary electrical and magnetic energy and to well-optimised non-magnetic baselines. In US-M studies, it is therefore prudent to treat the magnetic field primarily as a controllable flow field unless spin-dependent reaction pathways are explicitly isolated. Specific energy consumption should include the power required to generate both the magnetic and ultrasonic fields, with field strengths and acoustic power characterised following established ultrasound metrology practice [6,57].

Multi-field hybrid systems

Hybrid stacks combining electric, magnetic, ultrasonic and thermal fields (*e.g.* US-E-T, US-E-M, E-M-T) are increasingly proposed as "maximally intensified" electrolysers. To move from concept to defensible engineering guidance, such systems must be evaluated using structured evidence matrices that jointly consider configuration, field strengths, Δ-metrics and specific energy consumption (SEC), rather than only reporting a few favourable operating points.

From concept to evidence matrices

Multi-field stacks are best represented as configuration × field-intensity × Δ-metric × SEC matrices that explicitly include neutral and negative regimes. For ultrasound, this requires IEC-traceable delivered acoustic intensity at the electrode ($W \cdot cm^{-2}$), while co-fields are specified using experimentally controllable and reportable quantities, including electrochemical current density (j / $A \cdot cm^{-2}$) and cell voltage (V / V), magnetic flux density (B_{mag} / T), and bulk or local electrolyte temperature (T / K), with temperature gradients or offsets relative to the bulk explicitly reported as ΔT where relevant [6,12,85]. Recent work on flow-engineered three-dimensional electrodes and dual-layer flow fields already demonstrates strong bubble management and improved mass transfer without ultrasound, illustrating how much can be gained from purely geometrical and hydrodynamic optimization [95-97]. Hybrid E-M-US-T claims are persuasive only when they outperform such advanced non-acoustic baselines after full energy normalisation, including auxiliary pumping, magnet and ultrasound power. To avoid survivorship bias, multi-field studies should report not only the best-performing operating points but also the windows where benefits taper or reverse, so that design spaces can be compared across technologies on a consistent Δj, Δη, ΔHPR and SEC basis [95-97].

Diagnostics for fair comparison

Robust diagnostics are essential to disentangle how each field contributes to performance. Volumetric passive acoustic mapping (PAM/PCM/3D-PAM) and time-domain approaches such as PADAM or higher-order DMAS beamforming can co-register cavitation activity with the spatial distribution of electrodes and flow channels [75,87-90]. When paired with high-speed or ultrafast optical imaging, these tools can map bubble nucleation, growth and lift-off on architected electrodes and flow-engineered structures, linking local cavitation regimes to bubble detachment and mass-transfer patterns [75,82]. Alongside these acoustic and optical diagnostics, thermal maps under nominally isothermal control are needed to distinguish cavitation-driven enhancements from simple heating [85,91]. All claims should state delivered acoustic intensity, $W \cdot cm^{-2}$, with uncertainty, co-field intensities (B_{mag}, j, T), together with electrolyte composition and dissolved-gas content, and clear SEC boundaries indicating which auxiliaries are included in the energy balance [6,57,85].

Baselines and decision rules

Several non-acoustic strategies can already rival ultrasound in bubble removal and mass-transfer enhancement at low auxiliary power. Pressure-swing degassing in zero-gap alkaline cells, dual-layer and other flow-field redesigns, and surface texturing using superaerophilic/superaerophobic architectures provide strong benchmarks for gas removal and performance at high current density [95-98]. A rigorous multi-field hybrid claim should therefore demonstrate superiority over these non-acoustic baselines on SEC (kWh·kg^{-1} H_2) at matched hydrogen output, not only on instantaneous current or overpotential. Within such stacks, US-M couplings should be treated primarily as flow-control tools unless spin-selective reaction pathways are explicitly isolated, while US-T effects must be disentangled from passive heating via isothermal controls and transparent heat balances. Because combined fields may accelerate degradation of catalysts, membranes and seals, durability testing over at least 10-50 h with post-mortem analysis of coatings and components, together with an explicit uncertainty budget for acoustic power, hydrophone sensitivity, SEC and gas flow measurements, should be considered integral to any efficiency claim in multi-field hybrid systems [96-98]

Summary and design recommendations

Across US-E, US-T, US-M and multi-field hybrid configurations, this section has shown that ultrasound and co-fields can, within tuned operating windows, thin gas films, accelerate bubble detachment and enhance interfacial mass transport. At the same time, additional acoustic, thermal and magnetic inputs do not automatically guarantee a net energy benefit: performance gains can taper or even reverse once specific energy consumption (SEC), auxiliary power and durability are accounted for. Any credible assessment of ultrasound-assisted electrolysis must therefore balance local transport enhancements against system-level energy and reliability metrics.

On the basis of the recent literature, several design and reporting recommendations emerge:

(i) Adopt IEC-traceable acoustic metrology and consistent energy accounting, so that delivered acoustic intensity (W·cm^{-2}) and SEC (kWh·kg^{-1} H_2) are comparable across studies.

(ii) Represent operating spaces as response-surface maps rather than isolated best points, explicitly including neutral and negative regimes for frequency, duty cycle, temperature and co-field strengths.

(iii) Use real-time cavitation diagnostics (*e.g.* PAM/PCM/3D-PAM, PADAM/DMAS) co-registered with electrochemical and thermal measurements, to separate cavitation-driven effects from simple heating or hydrodynamic changes.

(iv) Treat US-M primarily as a controllable flow field unless spin-selective pathways are explicitly demonstrated, and disentangle US-T effects from passive heating using isothermal controls and transparent heat balances.

(v) Quantify durability and uncertainty: report degradation under combined fields (at least tens of hours where feasible), benchmark against non-acoustic baselines such as advanced flow-field and surface designs, and provide uncertainty budgets for acoustic power, field strengths, gas flow and SEC.

Taken together, these principles help close the loop between mechanistic understanding and system-level metrics. Multi-field synergy may enable more compact and higher-current-density electrolysers, but its practical value depends on whether it consistently delivers gains in hydrogen productivity and energy efficiency under realistic operating and lifetime constraints. Future work will therefore need to concentrate on systematically mapping multi-field design spaces, scaling experimentally validated concepts from laboratory cells to industrially relevant architectures, and

embedding acoustics and co-fields within techno-economic and sustainability assessments of green hydrogen production.

Conclusion

This review set out to organize recent work on ultrasound-assisted hydrogen production into a metrology-anchored, energy-normalized evidence base focused on sono-electrolysis. By aligning reporting with IEC-traceable acoustic measurements and explicitly defining energy boundaries, qualitative claims in the literature can be converted into quantitative outcomes that are comparable across laboratories and useful for engineering design and scale-up.

With respect to RQ1, which asked what level of performance gain can be reproduced under well-defined acoustic dosing, controlled isothermal studies where delivered acoustic intensity at the electrode is specified ($W \cdot cm^{-2}$) consistently report transport-level improvements clustering around $\Delta j \approx 15$ to 30 %, $\Delta \eta \approx 40$-120 mV, and ΔHPR ≈ 10 to 30 % within tuned operating windows. These gains largely vanish when geometry and stand-off are poorly documented, dissolved-gas control is absent, or temperature rise is not managed, indicating that ultrasound mainly acts by thinning boundary layers, accelerating bubble detachment, and refreshing electrode surfaces. Consequently, claims that substantially exceed these ranges should be supported by unusually detailed evidence on geometry, acoustic dose, and diagnostics before they are used as design references.

For RQ2, which concerned net energy benefits once auxiliaries are included, the available data indicate that when auxiliary loads are counted in the specific energy consumption (SEC, $kWh \cdot kg^{-1}$ H_2), operating windows around 20 to 40 kHz with delivered intensity of approximately 0.2 to 1.0 $W \cdot cm^{-2}$ and bulk temperatures near 20 to 35 °C can yield about 8 to 12 % improvement in SEC at matched hydrogen output. When the acoustic dose exceeds approximately 1.0-1.6 $W \cdot cm^{-2}$, non-uniform fields, cavitation cloud shielding, and additional heating often attenuate or reverse these benefits. This implies that standardized energy accounting, reported alongside Δ-metrics, is essential; otherwise, apparent rate gains risk being achieved at the cost of lower overall system efficiency.

Regarding RQ3, which asked what minimum reporting set is needed for fair benchmarking, this review identifies a core set of parameters that should be reported routinely. A practical minimum reporting set includes: acoustic frequency; waveform parameters (duty cycle, pulse repetition frequency, burst length); delivered acoustic intensity at the electrode ($W \cdot cm^{-2}$) with IEC 61161/IEC 62127-2 traceability and uncertainty; sonotrode-electrode stand-off and cell geometry; electrolyte properties such as pH and conductivity; dissolved-gas identity and concentration (DO/DGC); bulk temperature and run time (including ΔT); gas metrology with temperature and pressure correction; explicit SEC boundaries indicating which auxiliaries are included; and replicate numbers with basic statistics. Adopting this minimum reporting set would help convert isolated case studies into datasets that support cross-lab comparisons and model validation.

Across these questions, metrology and diagnostics emerge as central to the credibility and transferability of reported performance. Studies that combine traceable acoustic measurements with operando cavitation-electrochemistry and that document both positive and neutral or negative regimes provide results that are more likely to generalize. In parallel, fair baselines are as important as peak gains: pressure-swing de-bubbling, flow-field redesign, and surface texturing already deliver strong bubble management and mass-transfer enhancement at relatively low auxiliary power. Hybrid ultrasound-based approaches are therefore persuasive only when they outperform such non-acoustic baselines after appropriate normalization. Within multi-field stacks, US-M couplings are most consistently interpreted as flow-control tools unless spin-selective pathways are explicitly

demonstrated, while US-T effects must be separated from passive heating using isothermal controls and transparent heat balances. Durability under combined fields on the order of at least 10 to 50 h, together with post-mortem analysis of coatings, membranes and seals, and a quantified uncertainty budget for acoustic power, hydrophone sensitivity, SEC and gas-flow measurements, should be regarded as integral components of any efficiency claim.

In the near term, several specific priorities emerge. These include: (i) establishing quantitative shielding criteria tied to geometry and void fraction, so that the onset of cavitation cloud shielding and its impact on effective dose can be predicted; (ii) implementing routine operando co-registration of cavitation activity and electrochemical response, for example through passive acoustic mapping combined with high-speed imaging and *V-j-T*-HPR measurements; (iii) developing scale-aware models that couple compressible bubble dynamics with reactor acoustics and two-phase electrochemical CFD to bridge laboratory probes and industrial cells; (iv) generating durability datasets under combined electric, acoustic, thermal and magnetic fields, including post-test characterization of materials; and (v) translating laboratory Δ-metrics to stack- and plant-level SEC and levelized cost of hydrogen (LCOH) with explicit system boundaries and auxiliary loads.

In summary, the literature indicates that ultrasound provides its greatest leverage through boundary-layer and bubble management within well-defined operating windows, rather than through unlimited performance gains. If IEC-traceable acoustic metrology, a common minimum reporting set, and energy-normalized Δ-metrics are systematically adopted, ultrasound, alone or in combination with other fields, can move from case-specific demonstrations toward designable, scalable and auditable options within cost- and efficiency-constrained hydrogen supply chains.

List of abbreviations

US	Ultrasound	DO	Dissolved oxygen
HIUS	High-intensity ultrasound	PCD	Passive cavitation detection
AWE	Alkaline water electrolysis	PAM	Passive acoustic mapping
PEM	Proton exchange membrane	PCM/3D-PAM	Passive cavitation mapping / 3D passive acoustic mapping
HER	Hydrogen evolution reaction		
OER	Oxygen evolution reaction	PADAM	Passive acoustic dynamic differentiation and mapping
SEC	Specific energy consumption		
PV	Photovoltaic	DMAS	Delay-multiply-and-sum
US-E	Ultrasound-electric coupling	SCL	Sonochemiluminescence
US-T	Ultrasound-thermal coupling	IEC	International Electrotechnical Commission
US-M	Ultrasound-magnetic coupling	RFB	Radiation-force balance
E-M-US-T	Multi-field hybrid system	CFD	Computational fluid dynamics
CW	Continuous-wave ultrasound	MRS	Minimum reporting set
PU	Pulsed ultrasound	LCOH	Levelized cost of hydrogen
DGC	Dissolved-gas concentration	PRF	Pulse repetition frequency

***Conflict of interest**: The authors declare no conflict of interest.*

***Funding**: This research was funded by the Ministry of Higher Education Malaysia under the Fundamental Research Grant Scheme (FRGS), Project Code: FRGS/1/2023/TK08/USM/02/10.*

***AI Statement:** Artificial intelligence tools were used to polish language and improve clarity. All scientific content, interpretations and conclusions were conceived, verified and approved by the authors.*

References

[1] International Energy Agency, *Global Hydrogen Review 2024.* https://www.iea.org/reports/global-hydrogen-review-2024 (accessed September 24, 2025).

[2] R. F. Martínez, G. Cravotto, P. Cintas, Organic sonochemistry: A chemist's timely perspective on mechanisms and reactivity, *Journal of Organic Chemistry* **86** (2021) 13833-13856. https://doi.org/10.1021/acs.joc.1c00805
[3] S. Kwon, S. Bae, G. Son, Experimental study of ultrasound-assisted alkaline water electrolysis for hydrogen production, *Journal of Mechanical Science and Technology* **39** (2025) 663-669. https://doi.org/10.1007/s12206-025-0113-9
[4] Y. H. Teoh, S. Y. Liew, H. G. How, H. Yaqoob, M. Y. Idroas, M. A. Jamil, S. U. Mahmud, T. D. Le, H. M. Ali, M. W. Shahzad, Investigating sono-electrolysis for hydrogen generation and energy optimization, *International Communications in Heat and Mass Transfer* **164** (2025) 108980. https://doi.org/10.1016/j.icheatmasstransfer.2025.108980
[5] IEC 62127-2:2025, *International Electrotechnical Commission*. https://webstore.iec.ch/en/publication/68572 (accessed September 24, 2025)
[6] IEC 61161:2013, *International Electrotechnical Commission*. https://webstore.iec.ch/en/publication/4708 (accessed August 26, 2025)
[7] IEC TS 62462:2017, *Intertek Inform*. https://www.intertekinform.com/en-au/standards/iec-ts-62462-2017-561987_saig_iec_iec_2995392 (accessed September 9, 2025)
[8] S. Joshi, C. Agarkoti, P. R. Gogate, Mapping of 20 L capacity ultrasonic reactor using cavitation activity meter and dye degradation, *Ultrasonics Sonochemistry* **101** (2023) 106688. https://doi.org/10.1016/j.ultsonch.2023.106688
[9] D. Meroni, R. Djellabi, M. Ashokkumar, C. L. Bianchi, D. C. Boffito, Sonoprocessing: From concepts to large-scale reactors, *Chemical Reviews* **122** (2022) 3219-3258. https://doi.org/10.1021/acs.chemrev.1c00438
[10] P. Adamou, E. Harkou, A. Villa, A. Constantinou, N. Dimitratos, Ultrasonic reactor set-ups and applications, *Ultrasonics Sonochemistry* **107** (2024) 106925. https://doi.org/10.1016/j.ultsonch.2024.106925
[11] N. H. Merabet, K. Kerboua, Green hydrogen from sono-electrolysis: A coupled numerical and experimental study of the ultrasound assisted membraneless electrolysis of water supplied by PV, *Fuel* **356** (2024) 129625. https://doi.org/10.1016/j.fuel.2023.129625
[12] J. Gravelle, J. Y. Hihn, B. G. Pollet, Power ultrasound as performance enhancer for alkaline water electrolysis: A review, *International Journal of Hydrogen Energy* **100** (2025) 428-441. https://doi.org/10.1016/j.ijhydene.2024.12.243
[13] *Ultrasound power and radiation force balances*, National Physical Laboratory (NPL). https://www.npl.co.uk/products-services/ultrasound/radiation-force-balance (accessed September 6, 2025)
[14] I. Fernández-Osete, D. Bermejo, X. Ayneto-Gubert, X. Escaler, Review of the uses of acoustic emissions in monitoring cavitation erosion and crack propagation, *Foundations* **4** (2024) 114-133. https://doi.org/10.3390/foundations4010009
[15] C. E. Brennen, *Cavitation and Bubble Dynamics*, Cambridge University Press, Cambridge, United Kingdom, 2013. https://doi.org/10.1017/CBO9781107338760
[16] T. G. Leighton, R. E. Apfel, The Acoustic Bubble, *Journal of the Acoustical Society of America* **96** (1994) 2616. https://doi.org/10.1121/1.410082
[17] F. Foroughi, C. Immanuel Bernäcker, L. Röntzsch, B. G. Pollet, Understanding the effects of ultrasound (408 kHz) on the hydrogen evolution reaction (HER) and the oxygen evolution reaction (OER) on Raney-Ni in alkaline media, *Ultrasonics Sonochemistry* **84** (2022) 105979. https://doi.org/10.1016/j.ultsonch.2022.105979
[18] Y. Zhu, X. Zhu, I. Soyler, X. Pan, L. X. Liu, M. J. Bussemaker, Prediction of sonochemical activity based on dimensionless analysis and multivariate linear regression, *Ultrasonics Sonochemistry* **120** (2025) 107427. https://doi.org/10.1016/j.ultsonch.2025.107427

[19] K. Fattahi, G. Dodier, E. Robert, D. C. Boffito, Flow effects on sonochemical oxidation activity in a 20 kHz ultrasonic horn system, *Chemical Engineering Journal* **489** (2024) 151203. https://doi.org/10.1016/j.cej.2024.151203
[20] C. Hwang, I. Na, Y. Son, Sonochemical oxidation activity in 20-kHz probe systems: The effects of vessel shape, vessel wall thickness, and probe position, *Ultrasonics Sonochemistry* **121** (2025) 107519. https://doi.org/10.1016/j.ultsonch.2025.107519
[21] G. Viciconte, V. P. Sarvothaman, P. Guida, T. T. Truscott, W. L. Roberts, High-speed imaging and coumarin dosimetry of horn type ultrasonic reactors: Influence of probe diameter and amplitude, *Ultrasonics Sonochemistry* **119** (2025) 107362. https://doi.org/10.1016/j.ultsonch.2025.107362
[22] Lord Rayleigh, VIII. On the pressure developed in a liquid during the collapse of a spherical cavity, *The London, Edinburgh, and Dublin Philosophical Magazine and Journal of Science* **34** (1917) 94-98. https://doi.org/10.1080/14786440808635681
[23] J. B. Keller, M. Miksis, Bubble oscillations of large amplitude, *Journal of the Acoustical Society of America* **68** (1980) 628-633. https://doi.org/10.1121/1.384720
[24] T. J. Tiong, J. K. Chu, K. W. Tan, Advancements in acoustic cavitation modelling: Progress, challenges, and future directions in sonochemical reactor design, *Ultrasonics Sonochemistry* **112** (2024) 107163. https://doi.org/10.1016/j.ultsonch.2024.107163
[25] K. Yasui, Origin of the broad-band noise in acoustic cavitation, *Ultrasonics Sonochemistry* **93** (2022) 106276. https://doi.org/10.1016/j.ultsonch.2022.106276
[26] E. A. Neppiras, Acoustic cavitation series: Part one: Acoustic cavitation: An introduction, *Ultrasonics* **22** (1984) 25-28. https://doi.org/10.1016/0041-624X(84)90057-X
[27] A. G. Athanassiadis, Z. Ma, N. Moreno-Gomez, K. Melde, E. Choi, R. Goyal, P. Fischer, Ultrasound-responsive systems as components for smart materials, *Chemical Reviews* **122** (2021) 5165-5208. https://doi.org/10.1021/acs.chemrev.1c00622
[28] P. Peñas, Á. M. Soto, D. Lohse, G. Lajoinie, D. Van Der Meer, Ultrasound-enhanced mass transfer during the growth and dissolution of surface gas bubbles, *International Journal of Heat and Mass Transfer* **174** (2021) 121069. https://doi.org/10.1016/j.ijheatmasstransfer.2021.121069
[29] B. Jia, H. Soyama, Non-spherical cavitation bubbles: A review, *Fluids* **9** (2024) 249. https://doi.org/10.3390/fluids9110249
[30] A. B. Sieber, D. B. Preso, M. Farhat, Cavitation bubble dynamics and microjet atomization near tissue-mimicking materials, *Physics of Fluids* **35** (2023) 013306. https://doi.org/10.1063/5.0136577
[31] X. Lu, C. Chen, K. Dong, Z. Li, J. Chen, An equivalent method of jet impact loading from collapsing near-wall acoustic bubbles: A preliminary study, *Ultrasonics Sonochemistry* **79** (2021) 105760. https://doi.org/10.1016/j.ultsonch.2021.105760
[32] A. Kiyama, T. Shimazaki, J. M. Gordillo, Y. Tagawa, Direction of the microjet produced by the collapse of a cavitation bubble located in a corner of a wall and a free surface, *Physical Review Fluids* **6** (2021) 083601. https://doi.org/10.1103/PhysRevFluids.6.083601
[33] H. Su, J. Sun, C. Wang, H. Wang, Temperature impacts on the growth of hydrogen bubbles during ultrasonic vibration-enhanced hydrogen generation, *Ultrasonics Sonochemistry* **102** (2024) 106734. https://doi.org/10.1016/j.ultsonch.2023.106734
[34] A. Sahoo, H. He, D. Darrow, C. C. Chen, E. S. Ebbini, Image-guided measurement of radiation force induced by focused ultrasound beams, *IEEE Transactions on Ultrasonics, Ferroelectrics, and Frequency Control* **70** (2023) 138-146. https://doi.org/10.1109/TUFFC.2022.3221049
[35] P. Domenighini, F. Costantino, P. L. Gentili, A. Donnadio, M. Nocchetti, A. Macchioni, F. Rossi, F. Cotana, Future perspectives in green hydrogen production by catalyzed sono-photolysis of water, *Sustainable Energy and Fuels* **8** (2024) 3001-3014. https://doi.org/10.1039/D4SE00277F

[36] C. Pétrier, A. Francony, Ultrasonic waste-water treatment: Incidence of ultrasonic frequency on the rate of phenol and carbon tetrachloride degradation, *Ultrasonics Sonochemistry* **4** (1997) 295-300. https://doi.org/10.1016/S1350-4177(97)00036-9
[37] Y. Jiang, C. Petrier, T. D. Waite, Sonolysis of 4-chlorophenol in aqueous solution: Effects of substrate concentration, aqueous temperature and ultrasonic frequency, *Ultrasonics Sonochemistry* **13** (2006) 415-422. https://doi.org/10.1016/j.ultsonch.2005.07.003
[38] S. Merouani, O. Hamdaoui, Y. Rezgui, M. Guemini, Sensitivity of free radicals production in acoustically driven bubble to the ultrasonic frequency and nature of dissolved gases, *Ultrasonics Sonochemistry* **22** (2015) 41-50. https://doi.org/10.1016/j.ultsonch.2014.07.011
[39] H. N. McMurray, D. A. Worsley, B. P. Wilson, Hydrogen evolution and oxygen reduction at a titanium sonotrode, *Chemical Communications* (1998) 887-888. https://doi.org/10.1039/A800801I
[40] Y. Mizukoshi, H. Nakamura, H. Bandow, Y. Maeda, Y. Nagata, Sonolysis of organic liquid: Effect of vapour pressure and evaporation rate, *Ultrasonics Sonochemistry* **6** (1999) 203-209. https://doi.org/10.1016/S1350-4177(99)00012-7
[41] S. K. Mohapatra, M. Misra, V. K. Mahajan, K. S. Raja, A novel method for the synthesis of titania nanotubes using sonoelectrochemical method and its application for photoelectrochemical splitting of water, *Journal of Catalysis* **246** (2007) 362-369. https://doi.org/10.1016/j.jcat.2006.12.020
[42] S. H. Zadeh, Hydrogen production via ultrasound-aided alkaline water electrolysis, *Journal of Automation and Control Engineering* **2** (2014) 103-109. https://doi.org/10.12720/joace.2.1.103-109
[43] K. Kerboua, N. H. Merabet, Sono-electrolysis performance based on indirect continuous sonication and membraneless alkaline electrolysis: Experiment, modelling and analysis, *Ultrasonics Sonochemistry* **96** (2023) 106429. https://doi.org/10.1016/j.ultsonch.2023.106429
[44] M. Shestakova, M. Vinatoru, T. J. Mason, E. Iakovleva, M. Sillanpää, Sonoelectrochemical degradation of formic acid using Ti/Ta_2O_5-SnO_2 electrodes, *Journal of Molecular Liquids* **223** (2016) 388-394. https://doi.org/10.1016/j.molliq.2016.08.054
[45] R. Ji, R. Pflieger, M. Virot, S. I. Nikitenko, Multibubble sonochemistry and sonoluminescence at 100 kHz: The missing link between low- and high-frequency ultrasound, *Journal of Physical Chemistry B* **122** (2018) 6989-6994. https://doi.org/10.1021/acs.jpcb.8b04267
[46] A. Singh, A. S. K. Sinha, Intensification of photocatalytic decomposition of water by ultrasound, *Journal of Energy Chemistry* **27** (2018) 1183-1188. https://doi.org/10.1016/j.jechem.2017.08.001
[47] T. T. P. Pham, P. H. D. Nguyen, T. C. Hoang, H. T. L. Duong, T. M. L. Le, K. P. H. Huynh, P. T. D. Nguyen, D. V. N. Vo, Simultaneous production of gaseous fuels with degradation of Rhodamine B using a 40 kHz double-bath-type sonoreactor, *International Journal of Hydrogen Energy* **46** (2021) 9292-9302. https://doi.org/10.1016/j.ijhydene.2020.12.091
[48] J. Choi, S. Yoon, Y. Son, Effects of alcohols and dissolved gases on sonochemical generation of hydrogen in a 300 kHz sonoreactor, *Ultrasonics Sonochemistry* **101** (2023) 106660. https://doi.org/10.1016/j.ultsonch.2023.106660
[49] N. H. Merabet, K. Kerboua, Membrane free alkaline sono-electrolysis for hydrogen production: An experimental approach, *International Journal of Hydrogen Energy* **49** (2024) 734-753. https://doi.org/10.1016/j.ijhydene.2023.09.061
[50] J. Gravelle, V. Avramovic, L. Hallez, J. Y. Hihn, B. G. Pollet, Effects of a perpendicular ultrasonic field on planar and porous electrodes for hydrogen production in alkaline conditions, *Ultrasonics Sonochemistry* **120** (2025) 107481. https://doi.org/10.1016/j.ultsonch.2025.107481

[51] S. Merouani, A. Dehane, O. Hamdaoui, Hydrogen production via water ultrasonication: A review, *Ultrasonics Sonochemistry* **120** (2025) 107515. https://doi.org/10.1016/j.ultsonch.2025.107515
[52] A. Saad, L. Bai, F. M. S. Christensen, S. Luo, A. Bentien, M. Ashokkumar, Z. Wei, Ultrasound-enhanced alkaline water splitting with fast bubble release and sustained Ni catalysts, *Applied Catalysis B: Environmental and Energy* **370** (2025) 125152. https://doi.org/10.1016/j.apcatb.2025.125152
[53] M. Ashokkumar, J. Lee, Y. Iida, K. Yasui, T. Kozuka, T. Tuziuti, A. Towata, The detection and control of stable and transient acoustic cavitation bubbles, *Physical Chemistry Chemical Physics* **11** (2009) 10118-10121. https://doi.org/10.1039/B915715H
[54] F. Araújo, R. C. Neto, A. S. Moita, Alkaline water electrolysis: Ultrasonic field and hydrogen bubble formation, *International Journal of Hydrogen Energy* **78** (2024) 594-603. https://doi.org/10.1016/j.ijhydene.2024.06.263
[55] D. L. Parr IV, C. G. Duda, J. Leddy, Why sonochemistry in a thin layer? Constructive interference, *Journal of Physical Chemistry C* **127** (2023) 12184-12193. https://doi.org/10.1021/acs.jpcc.3c00804
[56] A. Angulo, P. van der Linde, H. Gardeniers, M. Modestino, D. Fernández Rivas, Influence of bubbles on the energy conversion efficiency of electrochemical reactors, *Joule* **4** (2020) 555-579. https://doi.org/10.1016/j.joule.2020.01.005
[57] G. R. Harris, S. M. Howard, A. M. Hurrell, P. A. Lewin, M. E. Schafer, K. A. Wear, V. Wilkens, B. Zeqiri, Hydrophone measurements for biomedical ultrasound applications: A review, *IEEE Transactions on Ultrasonics, Ferroelectrics, and Frequency Control* **70** (2023) 85-100. https://doi.org/10.1109/TUFFC.2022.3213185
[58] K. M. Cho, P. R. Deshmukh, W. G. Shin, Hydrodynamic behavior of bubbles at gas-evolving electrode in ultrasonic field during water electrolysis, *Ultrasonics Sonochemistry* **80** (2021) 105796. https://doi.org/10.1016/j.ultsonch.2021.105796
[59] H. Su, J. Sun, C. Wang, H. Wang, Study on the influence of ultrasound on the kinetic behaviour of hydrogen bubbles produced by proton exchange membrane electrolysis with water, *Ultrasonics Sonochemistry* **108** (2024) 106968. https://doi.org/10.1016/j.ultsonch.2024.106968
[60] K. Kerboua, O. Hamdaoui, Numerical estimation of ultrasonic production of hydrogen: Effect of ideal and real gas based models, *Ultrasonics Sonochemistry* **40** (2018) 194-200. https://doi.org/10.1016/j.ultsonch.2017.07.005
[61] A. Elmaihy, M. I. Amin, M. Bennaya, A. Rashad, Thermodynamic modeling of alkaline water electrolyzer and assessment of reported cell voltages correlations at low temperature and atmospheric pressure: Critical review, *Journal of Energy Storage* **96** (2024) 112674. https://doi.org/10.1016/j.est.2024.112674
[62] K. Peng, F. G. F. Qin, R. Jiang, S. Kang, Interpreting the influence of liquid temperature on cavitation collapse intensity through bubble dynamic analysis, *Ultrasonics Sonochemistry* **69** (2020) 105253. https://doi.org/10.1016/j.ultsonch.2020.105253
[63] Z. Kobus, M. Krzywicka, A. Starek-Wójcicka, A. Sagan, Effect of the duty cycle of the ultrasonic processor on the efficiency of extraction of phenolic compounds from *Sorbus intermedia*, *Scientific Reports* **12** (2022) 12244. https://doi.org/10.1038/s41598-022-12244-y.
[64] S. V. Sancheti, P. R. Gogate, A review of engineering aspects of intensification of chemical synthesis using ultrasound, *Ultrasonics Sonochemistry* **36** (2017) 527-543. https://doi.org/10.1016/j.ultsonch.2016.08.009
[65] C. N. Quiroz-Reyes, M. Á. Aguilar-Méndez, Continuous ultrasound and pulsed ultrasound: Selective extraction tools to obtain enriched antioxidants extracts from cocoa beans (*Theobroma cacao* L.), *Innovative Food Science and Emerging Technologies* **80** (2022) 103095. https://doi.org/10.1016/j.ifset.2022.103095

[66] R. A. Al-Juboori, T. Yusaf, L. Bowtell, Energy conversion efficiency of pulsed ultrasound, *Energy Procedia* **75** (2015) 1560-1568. https://doi.org/10.1016/j.egypro.2015.07.340.
[67] Y. Sun, X. Ye, Enhancement or reduction of sonochemical activity of pulsed ultrasound compared to continuous ultrasound at 20 kHz?, *Molecules* **18** (2013) 4858-4867. https://doi.org/10.3390/molecules18054858
[68] J. Choi, Y. Son, Effect of dissolved gases on sonochemical oxidation in a 20 kHz probe system: Continuous monitoring of dissolved oxygen concentration and sonochemical oxidation activity, *Ultrasonics Sonochemistry* **97** (2023) 106452. https://doi.org/10.1016/j.ultsonch.2023.106452
[69] S. Mukherjee, H. Gomez, Effect of dissolved gas on the tensile strength of water, *Physics of Fluids* **34** (2022) 126112. https://doi.org/10.1063/5.0131165
[70] J. Il Lee, B. S. Yim, J. M. Kim, Effect of dissolved-gas concentration on bulk nanobubbles generation using ultrasonication, *Scientific Reports* **10** (2020) 75818. https://doi.org/10.1038/s41598-020-75818-8
[71] S. Lee, Y. Son, Effects of gas saturation and sparging on sonochemical oxidation activity under different liquid level and volume conditions in 300-kHz sonoreactors: Zeroth- and first-order reaction comparison using KI dosimetry and BPA degradation, *Ultrasonics Sonochemistry* **98** (2023) 106521. https://doi.org/10.1016/j.ultsonch.2023.106521
[72] Y. Son, J. Seo, Effects of gas saturation and sparging on sonochemical oxidation activity in open and closed systems, Part I: H_2O_2 generation, *Ultrasonics Sonochemistry* **90** (2022) 106214. https://doi.org/10.1016/j.ultsonch.2022.106214
[73] J. Rooze, E. V. Rebrov, J. C. Schouten, J. T. F. Keurentjes, Dissolved gas and ultrasonic cavitation - A review, *Ultrasonics Sonochemistry* **20** (2013) 1-11. https://doi.org/10.1016/j.ultsonch.2012.04.013.
[74] K. Leonov, I. Akhatov, The influence of dissolved gas on dynamics of a cavitation bubble in an elastic micro-confinement, *International Journal of Heat and Mass Transfer* **196** (2022) 123295. https://doi.org/10.1016/j.ijheatmasstransfer.2022.123295
[75] H. Shinar, T. Ilovitsh, Volumetric passive acoustic mapping and cavitation detection of nanobubbles under low-frequency insonation, *ACS Materials Au* **5** (2024) 159-169. https://doi.org/10.1021/acsmaterialsau.4c00064
[76] H. A. S. Kamimura, S. Y. Wu, J. Grondin, R. Ji, C. Aurup, W. Zheng, M. Heidmann, A. N. Pouliopoulos, E. E. Konofagou, Real-time passive acoustic mapping using sparse matrix multiplication, *IEEE Transactions on Ultrasonics, Ferroelectrics, and Frequency Control* **68** (2021) 164-177. https://doi.org/10.1109/TUFFC.2020.3001848
[77] S. Bae, K. Liu, A. N. Pouliopoulos, R. Ji, E. E. Konofagou, Real-time passive acoustic mapping with enhanced spatial resolution in neuronavigation-guided focused ultrasound for blood-brain barrier opening, *IEEE Transactions on Biomedical Engineering* **70** (2023) 2874-2885. https://doi.org/10.1109/TBME.2023.3266952
[78] S. W. Ohl, E. Klaseboer, B. C. Khoo, Bubbles with shock waves and ultrasound, *Interface Focus* **5** (2015) 20150019. https://doi.org/10.1098/rsfs.2015.0019
[79] K. Maeda, A. D. Maxwell, T. Colonius, W. Kreider, M. R. Bailey, Energy shielding by cavitation bubble clouds in burst wave lithotripsy, *Journal of the Acoustical Society of America* **144** (2018) 2952. https://doi.org/10.1121/1.5079641
[80] K. Maeda, A. D. Maxwell, Controlling the dynamics of cloud cavitation bubbles through acoustic feedback, *Physical Review Applied* **15** (2021) 034033. https://doi.org/10.1103/PhysRevApplied.15.034033
[81] H. McKenzie, A. M. Esposito, H. D. Peterson, H. E. Miller, H. J. Stanford, *Hydrogen Shot: Water electrolysis technology assessment*. https://www.energy.gov/sites/default/files/2024-12/hydrogen-shot-water-electrolysis-technology-assessment.pdf (accessed September 9, 2025)

[82] Y. Luo, L. Wang, Q. Chen, Z. Wang, M. Zheng, Y. Hou, Elucidating the effect of the catalyst layer morphology on the growth and detachment of bubbles in water electrolysis via lattice Boltzmann modeling, *ACS Applied Materials and Interfaces* **17** (2025) 15499-15509. https://doi.org/10.1021/acsami.4c22527

[83] S. Park, A. Bashkatov, J. J. J. Eggebeen, S. Lee, D. Lohse, D. Krug, M. T. M. Koper, Combined effects of electrode morphology and electrolyte composition on single H2 gas bubble detachment during hydrogen evolution reaction, *Nanoscale* **17** (2025) 10020-10034. https://doi.org/10.1039/d5nr00234f

[84] S. Zhang, X. Cao, B. Wang, J. Wei, L. Zhou, J. Han, J. Yun, Application of high-frequency pulsed electrolysis technology in enhancing hydrogen production efficiency and energy saving potential analysis, *International Journal of Hydrogen Energy* **109** (2025) 684-693. https://doi.org/10.1016/j.ijhydene.2025.02.158

[85] L. P. Ferraz, E. K. Silva, Unraveling the thermal effects of high-intensity ultrasound: A practical guide to acoustic power determination and heat management, *ACS Omega* **10** (2025) 20277-20285. https://doi.org/10.1021/acsomega.4c11498

[86] S. Puteanus, T. Miličić, U. Feldmann, T. Vidaković-Koch, Efficiency improvement by pulsed water electrolysis: An unjustified hope, *International Journal of Hydrogen Energy* **113** (2025) 478-484. https://doi.org/10.1016/j.ijhydene.2025.02.348

[87] S. Therre, M. Fournelle, S. Tretbar, Optimization of 3D passive acoustic mapping image metrics: Impact of sensor geometry and beamforming approach, *Sensors* **24** (2024) 1868. https://doi.org/10.3390/s24061868

[88] N. Caso, K. Patel, T. Sun, Passive acoustic dynamic differentiation and mapping: A time-domain passive cavitation localization and classification approach, *bioRxiv* (2025). https://doi.org/10.1101/2025.04.08.647829

[89] C. M. Huber, N. Dorsch, H. Ermert, M. Vossiek, I. Ullmann, S. Lyer, Passive cavitation mapping for biomedical applications using higher order delay multiply and sum beamformer with linear complexity, *Ultrasonics* **153** (2025) 107653. https://doi.org/10.1016/j.ultras.2025.107653

[90] Y. Zhu, G. Zhang, Q. Zhang, L. Luo, B. Ding, X. Guo, D. Zhang, J. Tu, Real-time passive cavitation mapping and B-mode fusion imaging via hybrid adaptive beamformer with modified diagnostic ultrasound platform, *Ultrasonics* **142** (2024) 107375. https://doi.org/10.1016/j.ultras.2024.107375

[91] H. Geng, T. Chen, J. Chen, B. Huang, G. Wang, Temperature effects on single cavitation bubble dynamics under the free field condition: Experimental and theoretical investigations on water, *Ultrasonics Sonochemistry* **120** (2025) 107520. https://doi.org/10.1016/j.ultsonch.2025.107520

[92] Ö. Akay, A. Bashkatov, E. Coy, K. Eckert, K. E. Einarsrud, A. Friedrich, B. Kimmel, S. Loos, G. Mutschke, L. Röntzsch, M. D. Symes, X. Yang, K. Brinkert, Electrolysis in reduced gravitational environments: Current research perspectives and future applications, *NPJ Microgravity* **8** (2022) 56. https://doi.org/10.1038/S41526-022-00239-Y

[93] Ö. Akay, M. Monfort-Castillo, T. St Francis, J. Becker, S. Saravanabavan, Á. Romero-Calvo, K. Brinkert, Magnetically induced convection enhances water electrolysis in microgravity, *Nature Chemistry* **17** (2025) 1673–1679. https://doi.org/10.1038/S41557-025-01890-0.

[94] P. Vensaus, Y. Liang, J. P. Ansermet, G. J. A. A. Soler-Illia, M. Lingenfelder, Enhancement of electrocatalysis through magnetic field effects on mass transport, *Nature Communications* **15** (2024) 2867. https://doi.org/10.1038/s41467-024-46980-8

[95] F. Rocha, C. Georgiadis, K. Van Droogenbroek, R. Delmelle, X. Pinon, G. Pyka, G. Kerckhofs, F. Egert, F. Razmjooei, S. A. Ansar, S. Mitsushima, J. Proost, Proton exchange membrane-like alkaline water electrolysis using flow-engineered three-dimensional electrodes, *Nature Communications* **15** (2024) 7444. https://doi.org/10.1038/s41467-024-51704-z

[96] L. Wu, Z. Pan, S. Yuan, X. Shi, Y. Liu, F. Liu, X. Yan, L. An, A dual-layer flow field design capable of enhancing bubble self-pumping and its application in water electrolyzer, *Chemical Engineering Journal* **488** (2024) 151000. https://doi.org/10.1016/j.cej.2024.151000

[97] J. Bleeker, C. van Kasteren, J. R. van Ommen, D. A. Vermaas, Gas bubble removal from a zero-gap alkaline electrolyser with a pressure swing and why foam electrodes might not be suitable at high current densities, *International Journal of Hydrogen Energy* **57** (2024) 1398-1407. https://doi.org/10.1016/j.ijhydene.2024.01.147

[98] C. Zhang, Z. Xu, N. Han, Y. Tian, T. Kallio, C. Yu, L. Jiang, Superaerophilic/superaerophobic cooperative electrode for efficient hydrogen evolution reaction via enhanced mass transfer, *Science Advances* **9** (2023) eadd6978. https://doi.org/10.1126/sciadv.add6978